

The Role of 3D Printing Technology in Microengineering of Microneedles


Usanee Detamornrat, Emma McAlister, Aaron R. J. Hutton, Eneko Larrañeta, and Ryan F. Donnelly*

Microneedles (MNs) are minimally invasive devices, which have gained extensive interest over the past decades in various fields including drug delivery, disease diagnosis, monitoring, and cosmetics. MN geometry and shape are key parameters that dictate performance and therapeutic efficacy, however, traditional fabrication methods, such as molding, may not be able to offer rapid design modifications. In this regard, the fabrication of MNs using 3D printing technology enables the rapid creation of complex MN prototypes with high accuracy and offers customizable MN devices with a desired shape and dimension. Moreover, 3D printing shows great potential in producing advanced transdermal drug delivery systems and medical devices by integrating MNs with a variety of technologies. This review aims to demonstrate the advantages of exploiting 3D printing technology as a new tool to microengineer MNs. Various 3D printing methods are introduced, and representative MNs manufactured by such approaches are highlighted in detail. The development of advanced MN devices is also included. Finally, clinical translation and future perspectives for the development of MNs using 3D printing are discussed.

1. Introduction

3D printing is an additive manufacturing technology capable of rapidly producing 3D prototypes based on the deposition of materials in a layer-by-layer manner.^[1] The versatility and customizability of 3D printing allow for the manufacture of complex structures to be achieved with high accuracy and precision, such as; bespoke medical devices (e.g., implants and prostheses), personalized medicines (e.g., 3D printed tablets), and tissue and organ regeneration.^[2–10] In 2015, the US Food and Drug Administration (FDA) approved the use of the first 3D printed medicine, Spritam (levetiracetam), for oral administration to treat epilepsy.^[11,12] Spritam is a registered

U. Detamornrat, E. McAlister, A. R. J. Hutton, E. Larrañeta, R. F. Donnelly
School of Pharmacy
Queen's University Belfast
Medical Biology Centre
97 Lisburn Road, Belfast BT9 7BL, UK
E-mail: r.donnelly@qub.ac.uk

 The ORCID identification number(s) for the author(s) of this article can be found under <https://doi.org/10.1002/smll.202106392>.

© 2022 The Authors. Small published by Wiley-VCH GmbH. This is an open access article under the terms of the Creative Commons Attribution License, which permits use, distribution and reproduction in any medium, provided the original work is properly cited.

DOI: 10.1002/smll.202106392

trademark of the company Aprecia Pharmaceuticals, LLC., Ohio, USA. Recently, Triastek has received Investigational New Drug (IND) approval from the US FDA for T19, their first 3D printed drug product designed to treat rheumatoid arthritis.^[13] As a result of this approval, research into 3D printing for drug delivery has continued to rapidly expand, with several commercially available 3D printers emerging.^[14–19] More recently, 3D printing has shown its promising potential in the mass production of face masks and face shields in the middle of the 2020 global pandemic when these items were in high demand for protecting healthcare professionals in the fight against COVID-19.^[20,21]

Generally, the fabrication of complex structures by 3D printing involves the creation of a prototype in computer-aided design (CAD) software, which is subsequently exported as a standard tessellation

language (STL) file and sent to the 3D printer.^[16,22] The 3D printer's software divides the 3D model data into consecutive 2D slices to facilitate the fabrication of each structure in a layer-by-layer manner. Additionally, 3D scanners can also be used to record objects or body parts in the form of digital 3D images.^[23] Likewise, X-rays, magnetic resonance imaging (MRI) and computerized tomography (CT) scans produce 2D radiographic images that can be converted to digital 3D model files for the fabrication of personalized anatomical structures.^[1,2,6,24–28]

In recent years, the use of 3D printing technology to produce tailor-shaped MNs has gained great attention. MNs are a non-invasive device consisting of multiple micron-sized needles on a single patch, ranging most commonly in height from 25 to 2000 μm .^[29] Upon skin insertion, MNs create temporary microscopic channels in the epidermis to either deliver drug molecules via diffusion into the microcirculation or to collect interstitial fluid (ISF) for disease diagnosis and monitoring.^[30–33] As a drug delivery platform, MNs combine the patient-friendly benefits of a transdermal patch with the potential delivery capabilities of a hypodermic injection. The unique attribute of MNs is that they are strong enough to penetrate the resilient skin barrier, the *stratum corneum* (SC), sufficiently to enable access to the skin's rich microcirculation, yet are short and narrow enough to avoid stimulation with nerve fibers or puncture blood vessels that primarily reside in the dermal layer. Painless application is thus considered the principal benefit of MNs.^[34–36]

As a platform for diagnosis and monitoring, the collection of ISF by MNs is not only painless but also supports real-time sensing of biological analytes.^[37–39] In comparison with hypodermic needles, MNs offer several advantages. For instance, traumatic skin conditions can be minimized and bleeding after insertion completely avoided. In contrast to hypodermic needles, MNs are less likely to cause skin infections when applied on the skin appropriately, as they minimize microbial penetration through the skin.^[40] Furthermore, MNs can be used as an alternative to hypodermic needles for those who experience trypanophobia—fear of needles. Approximately 3.5% to 10% of the general population are affected by trypanophobia.^[41] It has been reported that there is an increased prevalence of trypanophobia in the younger population. The greatest prevalence was observed in children who are younger than 10 years old (>60% prevalence), followed by adolescents (20–50% prevalence) and 20–40 years old adults (20–30% prevalence), respectively.^[42] Another benefit of MNs is that they are simple use. Patients can self-apply a MN patch without any requirements for special instructions or additional tools.^[36,43]

Several studies have shown that 3D printing can produce MNs in a reproducible fashion with high resolution and quality.^[44–48] The fabrication of MNs by 3D printing allows the fast modification of key properties that play an important role on the performance of MNs. This includes needle height, tip-radius, base diameter, needle geometry, needle thickness, and needle density.^[47,48] The use of 3D printing is not limited to supporting the creation of customized MNs. It has been shown to diminish some disadvantages of MNs.^[49] For instance, the outer surface of MNs can be coated with an antibiotic drug using inkjet printing to prevent skin infections that may be caused by the MN-induced pore formation on the SC.^[32,50] In addition, most 3D printing methods fabricate MNs from polymers which the properties are tunable, biocompatible, and biodegradable.^[51–54] With its huge potential, 3D printing technology has become a new promising tool to help create novel designs, improve efficacy and increase the functionality of MNs.

After describing the different MN delivery strategies, this review focuses on the fabrication of MNs using different 3D printing methods (**Figure 1**). Representative examples of MNs produced by each method will be included. In addition, the development of medical devices based on the integration of 3D printed MNs with other technologies will also be described. At the end of the review, future perspectives based on the usage of 3D printing in MN fabrication will be discussed.

2. MN Delivery Strategies

MNs can be categorized into five main drug delivery strategies, namely solid (**Figure 2A**), coated (**Figure 2B**), dissolving (**Figure 2C**), hollow (**Figure 2D**), and hydrogel-forming (**Figure 2E**). The numerous drug delivery strategies reflect the extensive nature of research in this field.

The use of solid MNs, also known as the “poke with patch” approach, requires a two-step application process. Initially, a solid MN is applied to puncture the SC to create temporary micropores. The MN is then removed, and a conventional drug formulation is placed over the site of MN insertion, typically

in the form of a transdermal patch, cream or gel. The creation of micropores in the skin increases skin permeability and movement of drug molecules via passive diffusion. Solid MNs have been employed extensively for the transdermal delivery of macromolecules, such as insulin.^[55–57] The materials used to produce solid MNs are typically silicon, metals (e.g., stainless steel, titanium, tantalum, and nickel) and polymers (e.g., polycarbonate, polymethylmethacrylate, poly-lactic-co-glycolic acid (PLGA), polyglycolic acid (PGA), polylactic acid (PLA), a copolymer of methylvinylether and maleic anhydride (PMVE/MA), and photolithographic epoxy).^[30,31] Despite solid MNs being mechanically strong and providing satisfying outcomes for drug delivery, the inconvenience of a two-step application process is considered the main challenge associated with this drug delivery strategy. Furthermore, the micropores remain open only for a limited time resulting in incomplete delivery of the active substance. It has been reported that the skin treated by MNs recovered its barrier properties within 2 h.^[58]

As the name suggests, coated MNs or the “coat and poke” approach relies on coating the micro-projections of the MN with the drug formulation, and subsequent insertion of the coated MN into the skin. Drug deposition occurs through the dissolution of the coating after being applied to the skin.^[59] Coated MNs have been employed for the delivery of a number of different drug molecules and peptides, for example, salmon calcitonin,^[60] desmopressin,^[61] parathyroid hormone,^[62] bleomycin,^[63] and lidocaine.^[64] While this drug delivery strategy offers a more efficient route of transdermal drug delivery than that described for skin pre-treatment with solid MNs, a limitation of this strategy is the amount of drug formulation that can be coated onto the MN array itself. Owing to the small size of the needles, the loading capacity of such needles is small. With dosing limited to typically microgram quantities, coated MNs are typically restricted to high potency drug molecules and vaccines.^[65,66] In addition, the thickness of MNs post-coating with drug formulation possibly increases, reducing the sharpness of the MNs.^[67] As a result, the ability for these MNs to perforate the skin is minimized.

The use of dissolving MNs or the “poke and release” approach functions by incorporating the drug molecules within the structure of the MN. Following insertion into the skin and upon contact with the skin ISF, dissolution of the MNs and subsequent drug delivery occurs in a single step. In recent years, dissolving MN arrays have been fabricated primarily from FDA-approved biocompatible polymers. Materials that have been used to fabricate dissolving MNs are polyvinylpyrrolidone (PVP), polyvinyl alcohol (PVA), PLGA, hyaluronic acid, maltose, fibroin, carboxymethyl cellulose (CMC), chondroitin sulfate, dextran, chitosan, poly- γ -glutamic acid, and sugars.^[31] Given that the majority of polymers are water-soluble, dissolving MN arrays are particularly amenable to drugs with a more hydrophilic character.^[65] Dissolving MN arrays have been used to deliver a range of active substances, from small molecule drugs^[68–73] to large biomolecules,^[74–78] which showcases the ability of such a platform to enhance transdermal drug delivery. Besides, dissolving MNs can be used as a controlled drug delivery device as the dissolution rate depends on the polymer constituting the MNs. Another main advantage of dissolving MNs is that they dissolve completely in

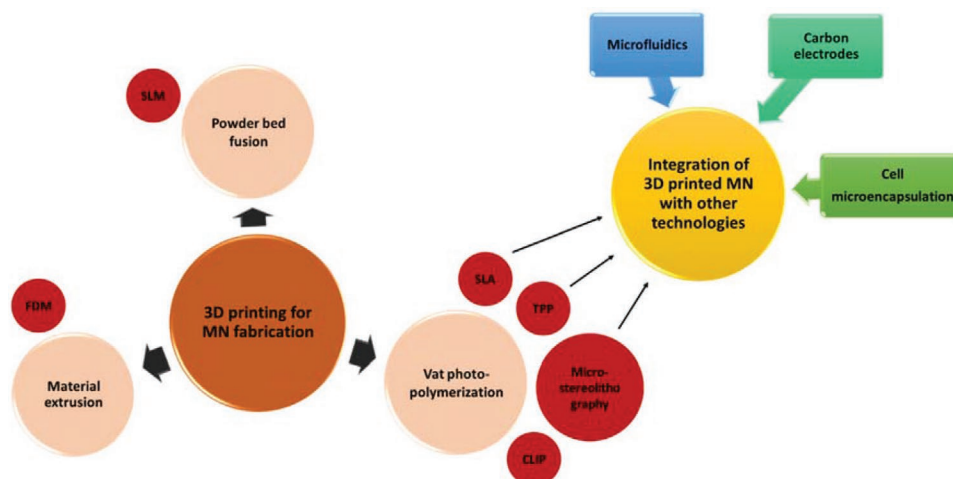


Figure 1. A schematic diagram of the key contents within this review. Various 3D printing methods classified by ISO/ASTM 52900 standard for additive manufacturing that have been utilized in the production of MNs are described. This includes material extrusion (FDM), vat photopolymerization (SLA, TPP, CLIP, and microstereolithography), and powder bed fusion (SLM). Additionally, this review also provides examples of devices fabricated by integrating the MNs produced by SLA, TPP, and microstereolithography 3D printing methods with microfluidics, carbon electrodes, or cell microencapsulation technologies.

the skin and therefore leave no sharp tips behind after use, reducing needle-stick injuries. Also, costs relating to sharp waste management can be avoided. The disadvantages of dissolving MNs include the limited amount of drug encapsulated in the MN matrix and possible non-uniform drug distribution in the polymer. The latter leads to inconsistencies in the dose

delivered to the skin. Moreover, it has been reported that dissolving MNs are hygroscopic and typically have low mechanical strength which prevents consistent and reliable penetration into the skin.^[79]

The use of hollow MN arrays or the “poke and flow” approach allows delivery of drug molecules via the injection of a fluid

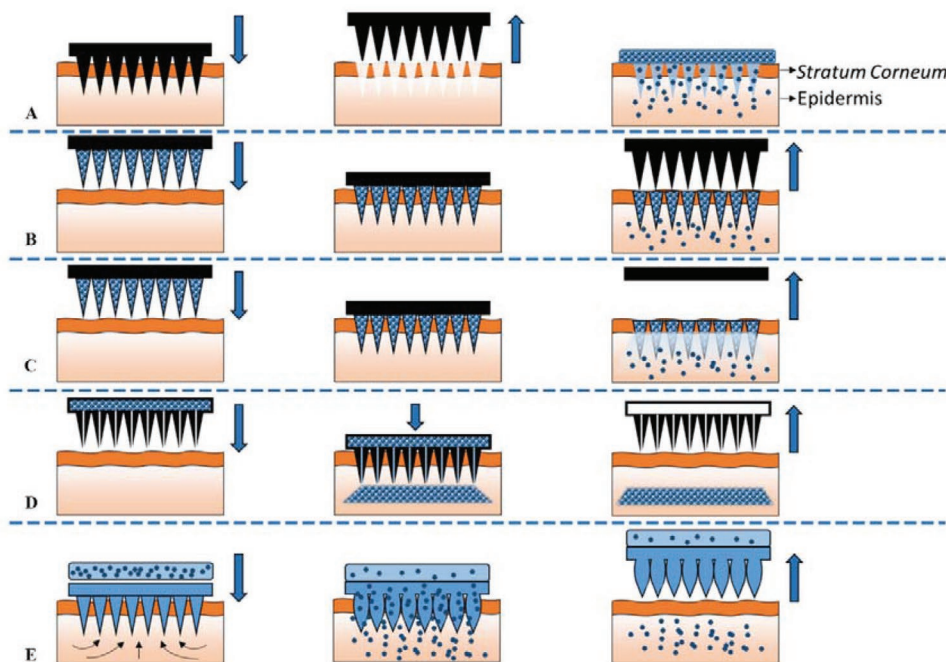


Figure 2. Five different types of MNs used for transdermal drug delivery. A) solid MNs that are applied to the skin to create transient micropores, followed by application of drug formulation, B) coated MNs for delivering drug that is coated on the surface of MNs. The release of drug is based on drug dissolution in the skin, C) dissolvable MNs for rapid or controlled release of drug that is incorporated in the water-soluble MNs, D) hollow MNs puncture the skin and enable the delivery of liquid drug formulation via active infusion or drug diffusion through the MN bores and E) hydrogel-forming MNs imbibe skin ISF upon the application, which subsequently induces the diffusion of drug in the reservoir through the swollen micro-projections to the skin. Reproduced with permission.^[30] Copyright 2016, Elsevier.

drug formulation through the central lumen of the hollow MNs into the skin. Hollow MNs facilitate continuous drug delivery by diffusion, pressure, or electrically driven flow of the active substance across the skin through the temporary pores created by the MNs.^[29] Hollow MNs are typically fabricated from silicon, metal, and glass.^[80–82] In comparison to solid or coated MNs, which are capable of delivering small quantities of drug molecules or peptides, this drug delivery strategy enabled the infusion of larger amounts of drug molecules.^[29] However, the successful use of hollow MNs can be hindered by potential clogging of the needle bore with tissue upon insertion, reducing potential drug delivery.

The use of hydrogel-forming or swellable MN arrays is the most recent drug delivery approach, first described by Donnelly et al.^[83] Following insertion into the skin, these MNs rapidly imbibe skin ISF and swell. As a result, continuous, unblockable, hydrogel conduits are formed. In this drug delivery strategy, the drug molecule is not within the hydrogel-forming MN array but in a separate drug-containing reservoir. The moisture from the swellable hydrogel-forming MN comes in contact with the attached drug-containing reservoir, causing it to dissolve/disintegrate. This subsequently triggers diffusion of the drug molecule from the attached drug-containing reservoir through the hydrogel matrix. Hydrogel-forming MN arrays have been shown to deliver various drug molecules and biopharmaceuticals of varying molecular weights.^[72,83–88] Hydrogel-forming MNs have been fabricated from polymers, which are crosslinked to form the hydrogel matrix.^[83–85] The most commonly used polymers for preparing hydrogel-forming MNs are Gantrez S-97, a copolymer of poly(methylvinylether-co-maleic acid) (PMVE/MA) crosslinked by esterification using polyethylene glycol,^[86] Gantrez AN-139, a copolymer of poly(methylvinylether-co-maleic anhydride) (PMVE/MAH) crosslinked with PEG,^[89] polystyrene-block-poly(acrylic acid) (PS-b-PAA),^[90] PLGA,^[91] PVA,^[92] crosslinked methacrylated hyaluronic acid (MeHA),^[93] and silk fibroin.^[94] Gantrez is a registered trademark of the company Ashland, Kidderminster, UK. As the drug is prepared in a separate drug-containing reservoir, the loading capacity is not linked to the MN array itself, removing any limitations on dosing. This is particularly useful for high dose drug molecules. Unlike coated or dissolving MNs, hydrogel-forming MNs release a drug from the drug reservoir located on the array after the needle section absorbs moisture from the skin. In general, the amount of drug that can be loaded on coated MNs is 1 and 37 mg for dissolving MNs.^[70] Since the drug reservoir is not part of MNs, drug loading is not restricted by the MN volume or surface area, unlike dissolving or coated MNs. Donnelly et al. highlighted this by showing that hydrogel-forming MNs could deliver up to 44 mg of ibuprofen to the skin.^[84] Similarly, Migdadi et al. reported that hydrogel-forming MNs can deliver metformin in the range of 50–75 mg to the skin.^[86] Courtenay et al. formulated lyophilized wafers containing 300 and 500 mg esketamine to be used with hydrogel-forming MNs.^[88] Due to such advantages, this novel technology has potential to increase the range of drug molecules that can be delivered transdermally. Developed in response to the challenges of the previously described drug-delivery strategies, this unique MN array design has its own advantages. Instead of transdermal drug delivery being primarily controlled by the barrier properties of the SC,

the control is now in the crosslink density of the hydrogel system. By altering the polymer crosslink density, the swelling rate of the hydrogel system can be controlled, thus conferring the ability to govern the drug release rate. This implies that drug delivery can be tailored on a case-by-case basis to meet the requirements of different drug molecules, thus confirming the versatility of this novel MN array design. Hydrogel-forming MN arrays are also removed from the skin completely intact. Therefore, no measurable polymer residue is left behind. Hydrogel-forming MN arrays are softened by the uptake of ISF, thus preventing reinsertion of the MN array. This reduces the risk of infection transmission that may arise from needle reuse.

In addition to their application in drug delivery, hydrogel-forming MNs have also been used for monitoring and diagnosis purposes. Owing to their ability to uptake skin ISF, imbibed ISF containing analytes in the MNs can be detected and quantified. Several studies have shown that hydrogel-forming MNs effectively uptook ISF from the site of application. The optimal application time is dependent on materials used to prepare MNs, analytes, and recovery methods. For example, Chang et al. used crosslinked MeHA MNs to extract skin ISF for 10 min. Approximately 1–10 μ L of ISF was collected, which was sufficient for glucose quantification.^[95] The clinical study conducted by Al-Kasasbeh et al. demonstrated that hydrogel-forming MNs prepared from an aqueous blend of 20% w/w PMVE/MA and 75% w/w polyethylene glycol (PEG) 10 000 Da were safe for human use since the MNs did not cause systemic reactions after repetitive application.^[96] The study also showed that the plasma concentrations of key biomarkers, including C-reactive protein (CRP), interleukin1- β (IL-1 β), tumor necrosis factor- α (TNF- α), immunoglobulin G (IgG), and immunoglobulin E (IgE) were comparable between pre- and post-MN application. Caffarel-Salvador et al. prepared MNs from an aqueous blend of 11.1% w/w hydrolyzed poly(methyl-vinylether-co-maleic anhydride) (PMVE/MAH) and 5.6% w/w PEG 10 000 Da which were then crosslinked by esterification.^[97] The in vitro study using excised neonatal porcine skin showed that theophylline, caffeine, and glucose uptaken by the MNs could be extracted from the MNs post-application (5 min). In addition, caffeine in the skin ISF of human volunteers could be extracted by the MNs post-consumption of 100 mg Proplus tablets. Proplus is a registered trademark of Lane Health Products Ltd, Gloucester, UK. After 1 h wearing time, the quantification of caffeine was performed by vortexing the MNs in HPLC water followed by HPLC analysis. The recovery of analytes or biomarkers is a straightforward process, which can be achieved by centrifugation or heating. However, heating is not suitable for proteinaceous biomarkers. He et al. suggested that a decrease in crosslink density between PVA and chitosan allows the recovery of biomarkers to be performed at lower temperature, thus avoiding protein denaturation.^[92] This solution could potentially be applicable with other polymers.

As mentioned previously, the type of MNs determines the materials used for MN production and defines the mechanism by which the active substance is released to the skin. However, MN type is not the only factor that influences the performance and therapeutic efficacy of MNs. Other parameters that should also be taken into consideration include geometry, shape, needle thickness, and needle density. In general, MNs ought to

penetrate into the skin without breaking or bending. Ideally, the optimal design should present a low insertion force and high fracture force. MN aspect ratio is defined as the ratio of the center-to-center interspacing between MNs to the MN radius.^[98] This parameter significantly affects the mechanical strength of MNs. Gittard et al. reported that decreasing the aspect ratio of a MN array led to an increase in its mechanical strength. MNs with the aspect ratio of 2:1 had a superior stiffness when compared to those with the aspect ratio of 3:1 (7500 N m⁻¹ vs 1620 N m⁻¹).^[99] Likewise, Davis et al. reported that increasing tip diameter and decreasing aspect ratio of MNs resulted in greater mechanical strength.^[100] Davidson et al. reported that the main parameters that significantly affect skin penetration were needle height and center-to-center interspacing between MNs.^[101] The study concluded that wider, longer, and more densely packed MNs lead to greater effective skin permeability.

Increasing the height of MNs is one of the approaches to provide more volume for drug loading and to achieve deeper skin penetration. As increasing the MN height reduces the distance that drug has to diffuse from the MN tips to the dermal microcirculation, resulting in an increase in the uptake of the drug by the dermal microcirculation. In terms of drug delivery, Donnelly et al. observed a significantly higher cumulative amount of theophylline delivered across the skin from an array with a needle height of 900 μm when compared to an array of 350 μm height MNs (292.23 ± 16.77 μg versus 242.62 ± 14.81 μg, *p*-value < 0.001).^[102] However, there is a limitation for this approach. The MNs with a height of greater than 1500 μm were found to trigger the nerve ending in the deeper dermis and cause pain. Gill et al. reported that 10 healthy volunteers (18–40 years old) perceived less pain upon the application of the MNs with shorter height (5% pain score for 480 μm height MNs versus 37% pain score for 1450 μm height MNs, *p*-value < 0.002).^[34] The greater density of MNs on the array results in a higher amount of drug encapsulated but it negatively affects the insertion capability of MNs. Because of less interspacing between MNs, the insertion force required for the array containing more MNs is increased, which possibly stimulates pain receptors. Gill et al. found that skin insertion with the array of 50 MNs resulted in a 2.5-fold increase in pain perception when compared to the array containing 5 MNs.^[34]

Loizidou et al. studied the effect of geometry on the skin penetration capability of MNs. The pyramidal MNs with three different base geometries including triangular, square, and hexagonal base were evaluated. Loizidou et al. observed that the penetration depth of the MNs with triangular base, square base, and hexagonal base were 340, 343, and 197 μm, respectively.^[103] The design of MNs with hexagonal base significantly inserted less than other designs (*p*-value < 0.01) because they withstand higher compressive stress and critical buckling loads than square and triangular MNs. Another study utilized an SLA 3D printer to produce two different designs, which were pyramidal and conical shapes MNs with 6 × 8 array, 1000 μm height, 1000 μm width, and 1.85 mm tip-to-tip interspacing. The conical MNs required less force to penetrate into the skin when compared to the pyramidal MNs.^[45] The adjustment of the maximum load required for penetration can attribute to the difference in the MN-to-skin contact area between pyramidal and conical MNs. Other shapes of MNs have also been investigated

(e.g., cross-shaped MNs), however, these shapes are less favorable due to complex fabrication processes, poor mechanical strength, and difficulties during removal from the skin.

In summary, the performance and therapeutic efficacy of MNs depend on the interplay of multiple parameters including geometries, shape, and drug loading. Various geometries and shapes can be simply generated using designing tools (e.g., CAD software). The challenge is therefore not how to design MNs but how to produce the MNs with optimal properties for skin insertion and drug release. These MNs should at least have strong mechanical strength to ensure that the MNs can penetrate into the skin without breakage. Adjusting the aspect ratio and fabricating the MNs with strong materials should avoid needle damages. In addition, the MNs must not cause pain during insertion, wearing, and removal in order to gain patients' compliance. To minimize pain, investigation of size and shape of MNs should be considered. To improve drug encapsulation and release mechanisms, other technologies can be integrated into the MNs. Extra accessories like a drug reservoir can be added to increase drug loading.

3. Use of 3D Printing Technology in the Fabrication of MNs

Herein, the fabrication of MNs will be discussed by dividing the methods of 3D printing into three groups which are based on the classification by ISO/ASTM 52900 standard for additive manufacturing. In each method, the principle and examples of fabricated MNs will be described. **Table 1** summarizes the examples of MNs fabricated by FDM, SLA, and TPP 3D printing methods and **Table 2** summarizes the examples of MNs fabricated by SLM, CLIP, and microstereolithography 3D printing methods.

3.1. Material Extrusion

3.1.1. Fused Deposition Modeling (FDM)

FDM is the most affordable 3D printing method and consequently the most accessible and widespread employed by researchers.^[124] The FDM method is based on hot-melt extrusion of thermoplastic polymer filament at the print head.^[1,14,22,125,126] While the movement of print head follows the pattern in 2D slice, the polymer filament is being extruded and deposited on the print station simultaneously.^[14,22,125,127] The repetition of such process results in the formation of a 3D structure, which is built vertically by the fusion between the former and the latter polymer layers. Once the temperature is below the melting point of the polymer, the 3D structure is hardened and ready for the removal from the print station.

To date, this printing method has been used to prepare solid MNs.^[104] The key advantage of FDM is that a wide range of thermoplastic polymers can be used such as poly(lactic acid) (PLA), acrylonitrile butadiene styrene, nylon, thermoplastic polyurethane, glycol-modified version of polyethylene terephthalate, polyether ether ketone, and polyetherimide.^[14,22,126,128,129] However, the surface of objects printed by FDM method is

Table 1. Examples of MNs fabricated by FDM, SLA, and TPP 3D printing technology.

Fabrication method	Conjunct technology	Material(s)	Design	Application(s)	Refs.
FDM	Chemical etching	PLA	Cylindrical MNs	Drug delivery	Luzuriaga et al. ^[104]
SLA	Micromolding	Resin for master MNs; carboxymethyl cellulose for MNs	Conical MNs	Drug delivery	Krieger et al. ^[48]
SLA	Isotropic shrinkage technique	RGD 720 resin for master MNs; Polyvinylpyrrolidone for MNs	Slanted-needle arrays	Drug delivery	Ochoa et al. ^[105]
SLA	Inkjet printing	Class I biocompatible resin	Conical and pyramidal MNs	Insulin delivery	Pere et al. ^[45]
SLA	Inkjet printing	Class I biocompatible resin	Pyramidal and flat spear- shaped MNs	Insulin delivery	Economidou et al. ^[106]
SLA	Inkjet printing	Class I biocompatible resin	Cross-shaped MNs	Drug delivery for anti-cancer drug	Uddin et al. ^[107]
SLA	–	AnyCubic colored resin	Triangular pyramidal MNs	Drug delivery	Lopez-Ramirez et al. ^[108]
TPP	–	Ormocer	Conical MNs	Medical devices	Doraiswamy et al. ^[109]
TPP	–	Ormocer	Hollow MNs	Drug delivery and ISF collection	Ovsianikov et al. ^[110]
TPP	Micromolding	Polyethylene glycol (200) and irgacure 369 for master MNs; eShell 200 for MNs	Conical MNs	Insulin delivery	Gittard et al. ^[111]
TPP	Micromolding and pulsed laser deposition	SR 259 polyethylene glycol dimethacrylate and irgacure 369 for master MNs; Ormocer for MNs	Cylindrical MNs with conical tips	Drug delivery for antibacterial agent	Gittard et al. ^[112]
TPP	Micromolding	Polyethylene glycol 600 diacrylate	Cylindrical MNs with conical tips	Drug delivery for antibacterial agent	Gittard et al. ^[113]
TPP	Iron sputtering deposition	Photoresist	Magnetic MNs in cylin- drical, pyramidal, and conical shapes	Drug delivery, tissue engineering, and single-cell analysis	Kavaldzhiev et al. ^[114]
TPP	–	IP-S photoresist	Hollow MNs	Drug delivery	Moussi et al. ^[115]

visibly not smooth due to low resolution and poor dimensional accuracy.^[126,127,130,131] In comparison with other common 3D printing methods, FDM has the lowest printing resolution.^[1] The additional postprocessing steps are required to smoothen the surface.^[127,131] Moreover, the objects produced by FDM are inherently anisotropic as the strength is not uniform throughout the structure.^[128,132–134] Due to the limitation of printer resolution, Luzuriaga et al. has shown that PLA MNs with fine details could not be reproducibly manufactured by FDM printing alone.^[104] The inaccurate formation of needles was a result of poor adhesion between PLA layers. Consequently, they produced PLA cylindrical shapes using FDM 3D printing instead (**Figure 3**). Such PLA cylindrical shapes were turned into MNs using post-fabrication chemical etching. This was achieved by allowing the cylindrical parts to immerse in potassium hydroxide (KOH) solution for different durations. The MNs with the tip diameters in the range of 1–55 μm were obtained while the length remained unchanged. The width of MNs, however, reduced by half of their original. The uniformity of the MNs could still be further improved as it would affect the performance and accuracy of drug loading per patch.

3.2. Vat Photopolymerization

3.2.1. Stereolithography (SLA)

The SLA method, developed by 3D Systems, Inc. in 1988, is based on photopolymerization of liquid resin in a vat using a UV laser beam.^[22,135] The UV laser beam is focused and scanned to trace a pattern on the surface of liquid resin.^[22,136,137] As a consequence, liquid resin is selectively cured and solidified after UV exposure. When the fabrication of the first layer is completed, the built platform is lowered to allow fresh liquid resin to cover the previous layer. The UV light-induced photopolymerization to fabricate the next layer out of liquid resin then begins. After the printing, the objects require an additional cleaning step to remove uncured resin.^[135] Thereafter, the mechanical strength of the objects is improved by the exposure to UV light.^[135,137–139]

The application of SLA in the production of MNs has been explored in numerous studies. Considering different method capacities, SLA supports the early-stage development of MNs by allowing the fast modification of MN prototypes to be

Table 2. Examples of MNs fabricated by SLM, CLIP, and microstereolithography 3D printing methods.

Fabrication method	Conjunct technology	Material(s)	Design	Application(s)	Reference
CLIP	–	Trimethylolpropane triacrylate and diphenyl (2,4,6-trimethylbenzoyl) phosphine oxide; Polyethylene glycol dimethacrylate; polycaprolactone trimethacrylate; acrylic acid	Square pyramidal MNs, arrowhead MNs, tiered MNs; and turret MNs	Drug delivery	Johnson et al. ^[47]
Microstereolithography	–	3DM-CAST resin	MN splints	Drug delivery	Lim et al. ^[116]
Microstereolithography	–	Polyethylene glycol diacrylate (PEG400DA)	Conical MNs	Drug delivery and ISF collection	Yao et al. ^[117]
Microstereolithography	–	Resin	MNs with quadrangular pyramid tip and square pillar basement	Drug delivery	Choi et al. ^[118]
Microstereolithography	Pulsed laser deposition	eShell 200	Flat conical MNs	Drug delivery for anti-bacterial agent	Gittard et al. ^[119]
Microstereolithography	–	Poly(propylene fumarate) and resin	Cylindrical MNs with conical tips	Drug delivery	Yun and Kim ^[120]
Microstereolithography	–	Poly(propylene fumarate)/diethyl fumarate	Cylindrical MNs	Delivery of chemotherapeutic drug	Lu et al. ^[121]
Microstereolithography	Micromolding and inkjet printing	eShell 200 for master MNs; Gantrez AN-139 for MNs	MNs with cylindrical base and conical shaped tip	Delivery of quantum dots	Boehm et al. ^[122]
Microstereolithography	Micromolding and inkjet printing	eShell 200 for master MNs; Gantrez AN-169 BF for MNs	Pyramidal-like MNs	Drug delivery for quantum dots as an anti-bacterial agent	Boehm et al. ^[50]
Microstereolithography	–	Polyethylene glycol 600 diacrylate	MNs with backward-facing barbs	Drug delivery	Han et al. ^[49]
SLM	–	Stainless steel 316L	Hollow MNs	Drug delivery	Gieseke et al. ^[123]

achieved in the desired dimension and shape. Moreover, SLA is perceived as a new effective tool to produce MN molds, which can be subsequently used in the fabrication of the various MN types.^[22] Typically, MN mold fabrication is carried out in the clean room using microfabrication approaches, such as photolithography and ultraviolet lithography.^[140–145] These approaches, however, are considered time-consuming and expensive, resulting in high cost of production.^[48,144] In this regard, SLA is a useful tool to fabricate on-demand master MN molds without the need of clean room. As a result, less expensive and faster production of MNs could be achieved, potentially promoting the mass production of MNs in the future.

SLA 3D printing has been used extensively for the fabrication of solid MNs. The first SLA-based MN fabrication was reported by Ochoa et al.^[105] The master solid MN was fabricated by SLA 3D printing and subsequently used as a template for casting agarose gel. The isotropic shrinkage of agarose gel preserved the structure of the MN. Subsequently, the dried agarose gel was used as a mold to produce MNs out of polydimethylsiloxane (PDMS) polymer. The study found that by coupling SLA 3D printing with the isotropic shrinkage of a hydrogel, the resolution of MNs was improved by at least fivefold when compared to the fabrication of MNs by SLA only. In addition, PDMS molds can be generated using the template of PDMS MNs. In this study, the authors demonstrated that polyvinylpyrrolidone (PVP) MNs fabricated by using the PDMS molds possessed the

tip radius of 9.6 μm , which were adequately sharp to penetrate porcine skin.

The appearance and mechanical strength of SLA 3D printed-MNs could be improved by adjusting the thickness in the Z-direction of each 2D slice and the aspect ratio of MNs, respectively. Krieger et al. observed that the fabrication of solid MNs with thinner layers reduced stair-stepping defect, resulting in a smoother surface of MNs when compared to those produced with thicker layers.^[48] Nevertheless, the printing time was prolonged as the number of slices increased. The aspect ratio was an important parameter impacting the mechanical strength and hence the skin penetration depth of the MNs. Insertion of higher aspect ratio MNs to the skin was easier, while lower aspect ratio MNs were mechanically stronger.

Krieger et al. introduced the “print and fill” technique for producing customized MN molds (**Figure 4**). SLA 3D printing was performed to fabricate a master solid MN. After printing, the basin in the MN was filled with different amounts of photocurable resin in order to create different MN heights. The greater the amount of resin poured into the basin, the shorter the MNs and vice versa. While, using the master MN with wider needle-to-needle distances increased the height of MNs when the equivalent amount of resin was filled in the basin. Following the curing by UV light, the master MN was subsequently used to produce silicone MN molds using the micromolding technique. This study demonstrated that the silicone molds were

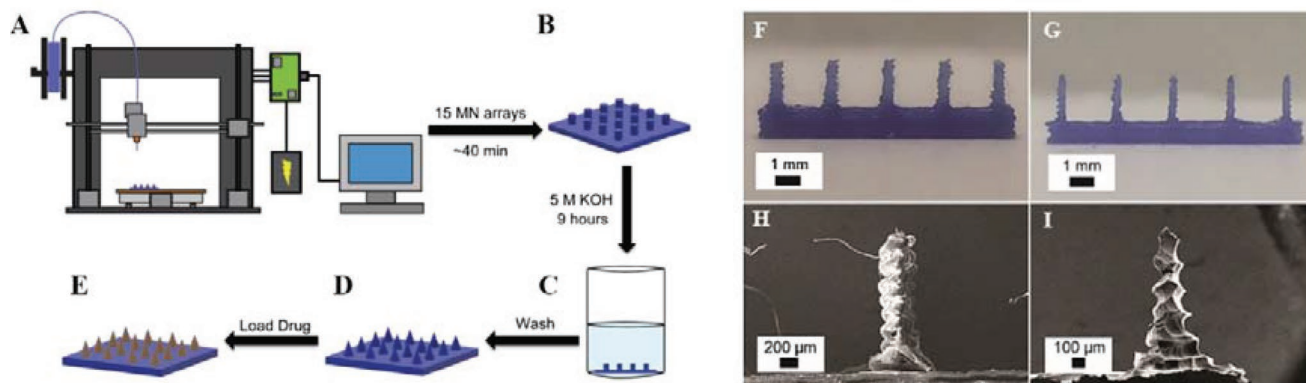


Figure 3. A–E) A schematic illustration of the fabrication of MNs by FDM 3D printing and chemical etching; optical images of F) MNs as FDM-fabricated; G) after etching in KOH solution; SEM images of H) MNs as fabricated and I) after etching in KOH solution. Adapted with permission.^[104] Copyright 2018, RSC.

versatile to the fabrication of MNs using different materials and methods; for example, carboxymethyl cellulose (CMC)-solvent casting method and PLA-thermal molding method.

All previous examples have involved the fabrication of a master solid MN using SLA 3D printing for the subsequent fabrication of MNs using the micromolding technique. SLA 3D printing has also been used in the fabrication of coated MNs. For example, Pere et al. coupled SLA 3D printing and inkjet printing to produce insulin-coated MNs.^[45] Pyramidal and conical MNs were fabricated by SLA 3D printing and their surfaces were subsequently coated by insulin blended with one of the stabilizers (trehalose, xylitol, and mannitol) in the ratio of 1:5 using inkjet printing. Based on picoliter pipetting in several jetting cycles, the total of 10 UI or 350 μg of insulin was accurately coated onto the surface of the needles present in the MN array. The in vitro release of insulin from the MNs was rapid with approximately 57–69% of insulin released within the first 5 min regardless of needle shape. Within an hour, approximately 90–95% of insulin was delivered across the skin. Further studies were employed by Economidou et al.^[106] In this study, pyramidal and flat spear-shaped MNs were fabricated using SLA 3D printing (Figure 5). Similar to the previous study, the outer surface of MNs was accurately coated with 10 UI (or 350 μg) of insulin using inkjet printing. Regarding the pyramidal-shaped MNs, more than 80% of insulin coated on the surface was rapidly released within 8 min in the in vitro study. Regarding the flat spear-shaped MNs, the in vitro release of insulin was slower due to their smaller surface area. Nonetheless, the sustained release of insulin from these MNs resulted in a steady hypoglycemic effect in streptozotocin-induced diabetic rats. The plasma glucose concentration in diabetic rats treated by insulin-coated MNs was comparable to those rats treated by subcutaneous injection of insulin at the same dose. The use of SLA coupled with inkjet printing was also observed in the study by Uddin et al.^[107] In this work, cisplatin-coated MNs were produced for skin cancer treatment. The cross-shaped MNs were fabricated from resin by SLA and accurately coated with drops of cisplatin embedded in hydrophilic polyvinyl caprolactame-polyvinyl acetate-polyethylene glycol polymer using a piezoelectric dispenser (Figure 6). The cross-shaped MNs showed a penetration depth of more than 80% of their length in

neonatal porcine skin and rapidly released approximately 80–90% of cisplatin within 1 h. The in vivo study in Balb/c nude mice showed that the MNs could provide sufficient cisplatin levels to effectively exhibit anticancer activity.

Lopez-Ramirez et al. used SLA 3D printing to fabricate a positive MN mold, which was subsequently used for producing a PDMS negative MN mold.^[108] The array of MNs was spatially separated to create different sections of active and passive MNs (Figure 7). The active MNs were designed to provide a rapid burst release of drug, using magnesium microparticles as a trigger reagent. While the passive MNs were designed for slow, sustained drug release. Within the same MN patch, different polymers and drugs can be used to create a combinatorial MN patch, which is proved effective to enhance immune response and longer survival in the in vivo studies using a B16F10 mouse melanoma model.

SLA has proved very useful and effective to manufacture customized MNs. These MNs have a smoother surface and intricate details when compared to those produced by FDM 3D printing. Therefore, they offered a good performance on skin insertion, which is one of the critical properties of MNs. As the geometry of MNs is easily tunable by modifying the structure in the CAD file before printing, it significantly reduces cost and time during research and development stage. The information of different designs and parameters used during printing can be easily collected and pooled for future development. In addition, mass production of MNs is possible by producing molds from SLA-generated master MNs. The molds enable the use of other polymers rather than only resin materials, including water-soluble polymers and biocompatible polymers. Therefore, the concern about the toxicity of some resins needed for SLA is alleviated. There are several examples that showed the capability of SLA-printed MNs as a drug carrier (e.g., anticancer drug)/protein carrier (e.g., insulin). Due to the fact that SLA 3D printed MNs have smooth and uniform surfaces, this allows the surface modification to be manipulated by dropping drug/protein solution on the defined area of MN surfaces. As a result, specific dose and regimen can be reliably delivered to the patients. The last example has emphasized the potential of SLA to design and produce a more complex MN array than usual. By adding a wall between sections, different zones were created

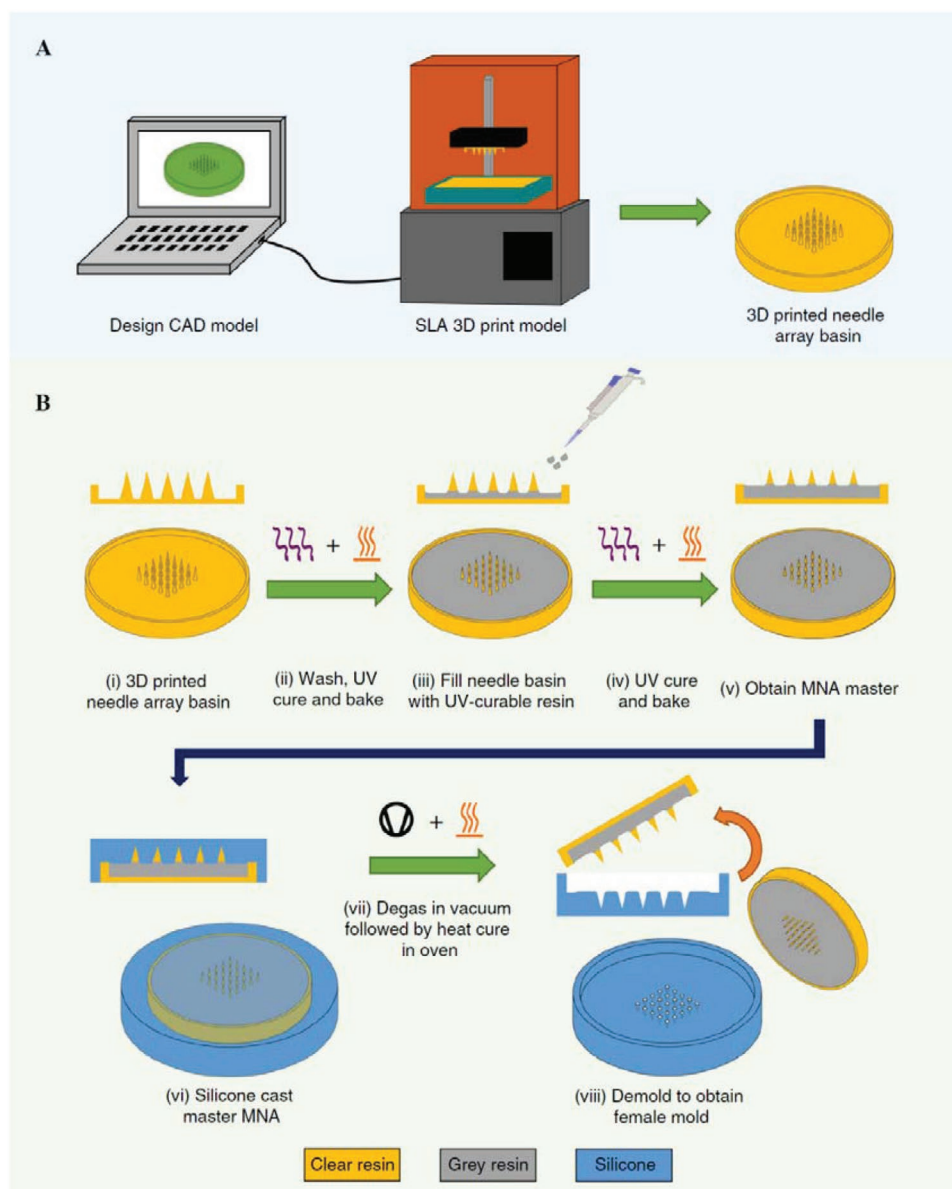


Figure 4. Overview of the “Print & Fill” fabrication method. A) needle array basin design followed by 3D printing of the design using a Form 2 SLA printer and B) MN master mold fabrication method in step i to viii. Reproduced with permission.^[48] Copyright 2019, Springer Nature.

and used to serve as different drug release profiles. Overall, the production of MNs by SLA can be improved further in both physiological properties and functionality. This is not limited to the application in drug delivery. It was believed that SLA 3D printing will play an important role in the fabrication of MNs for the application in some other areas, for example, disease monitoring. The main limitation of SLA is that it requires photoinitiators to facilitate photopolymerization.^[146–149] Residual photoinitiator remained in the printed objects and uncured resin are potentially cytotoxic. Meanwhile, SLA brings about a safety concern due to potential toxic chemicals; the material of choice to be used in FDM, on the other hand, is more versatile, hence toxic materials can be avoided. Table 3 provides toxicological information on the most commonly used photoinitiators, photopolymers and UV-curing agent. Several

studies showed that commercially available resins have cytotoxic effects in various models.^[150–152] The MTT viability assay showed that High Temp, Clear, Dental SG, Dental LT, Black and Flexible resins from Formlabs (Somerville, MA, USA) significantly reduced cell viability of human mesenchymal stem cells (p -value < 0.0001 for all but p -value < 0.001 for Dental SG).^[153] Clear and Dental SG resins also showed cytotoxic effects in gingival fibroblasts and L929 cells in MTT cell viability assay.^[154]

3.2.2. Two-Photon Polymerization (TPP)

TPP is the fabrication method involving photochemical reactions induced by spatial and temporal overlap of photons.^[156] TPP consists of three processes: initiation, propagation, and

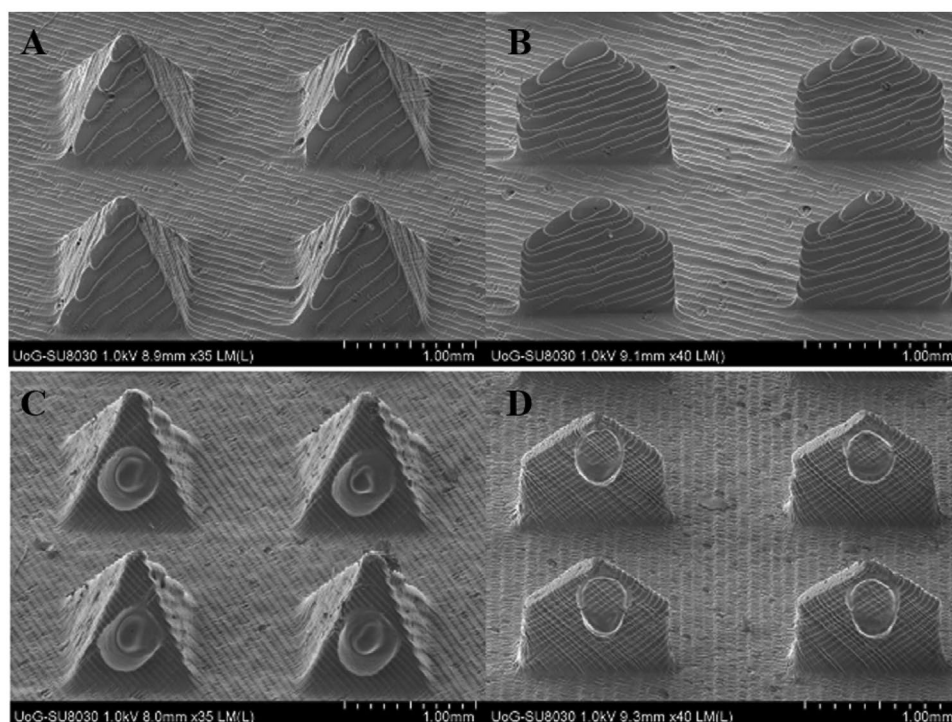


Figure 5. SEM images of the 3D printed MNs. A) Uncoated pyramid; B) uncoated spear; C) coated pyramid; D) coated spear. The thin films of insulin and xylitol (5:1) on the MNs were coated using an inkjet printer. Reproduced with permission.^[106] Copyright 2019, Elsevier.

termination.^[157] The initiation process involves the cleavage of chemical bonds with photoinitiator molecules by a femtosecond laser beam, which focuses into the small volume of the photosensitive resins by a high-numerical-aperture microscope objective. In this step, the photoinitiators are excited, and then decompose to radical species. In the propagation process, these radical species interact with monomers to generate monomer radicals. The termination process is when two monomer radicals combine together, ending the polymerization.

TPP has been typically used for the fabrication of hollow MNs. The first MNs produced by TPP were reported by Doraiswamy et al.^[109] These hollow MNs (750 μm height and 200 μm base diameter) were produced from organic–inorganic hybrid materials in which the organic part is made from a mixture of photosensitive siloxanes and biocompatible organic monomers with other additives such as a photoinitiator; while the inorganic part consists of ceramics or glasses. Such materials are known as organic-modified ceramics or Ormocer.^[22] Ormocer is a registered trademark of Fraunhofer

ISC, Würzburg, Germany. These MNs showed the ability to penetrate porcine skin without fracture and could support the proliferation of HT1080 epithelial-like cells as similar to polystyrene and extracellular matrix. In the following year, Ovsianikov et al. showed the feasibility of using femtosecond laser TPP to rapidly produce hollow MNs (Figure 8).^[110] MNs were again fabricated from Ormocer but contained 25 needles with the geometries of 800 μm height, 150–300 μm base diameter, and 500 μm needle-to-needle distance. This study highlighted that the off-center positions of the channels relative to the tip led to sharper MNs. Therefore, less force was required to insert the MNs into the skin. The hollow MNs were biocompatibility with human epidermal keratinocytes, highlighting a promising approach for drug delivery or ISF collection.

More recently, Moussi et al. used TPP to produce hollow MNs connected to a drug reservoir in a single step.^[115] The addition of a drug reservoir to the back of the MN increased the amount of drug delivered to the skin through the channels of the MNs. Four different MNs (200–400 μm height, 80–120 μm

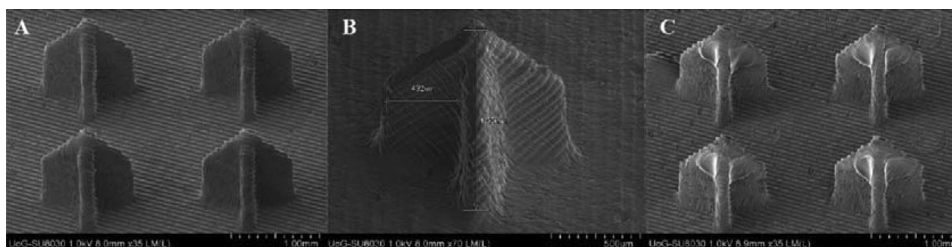


Figure 6. SEM images of A,B) uncoated 3D printed MNs at various magnifications and C) coated 3D printed cross-MNs. Reproduced with permission.^[107] Copyright 2020, Elsevier.

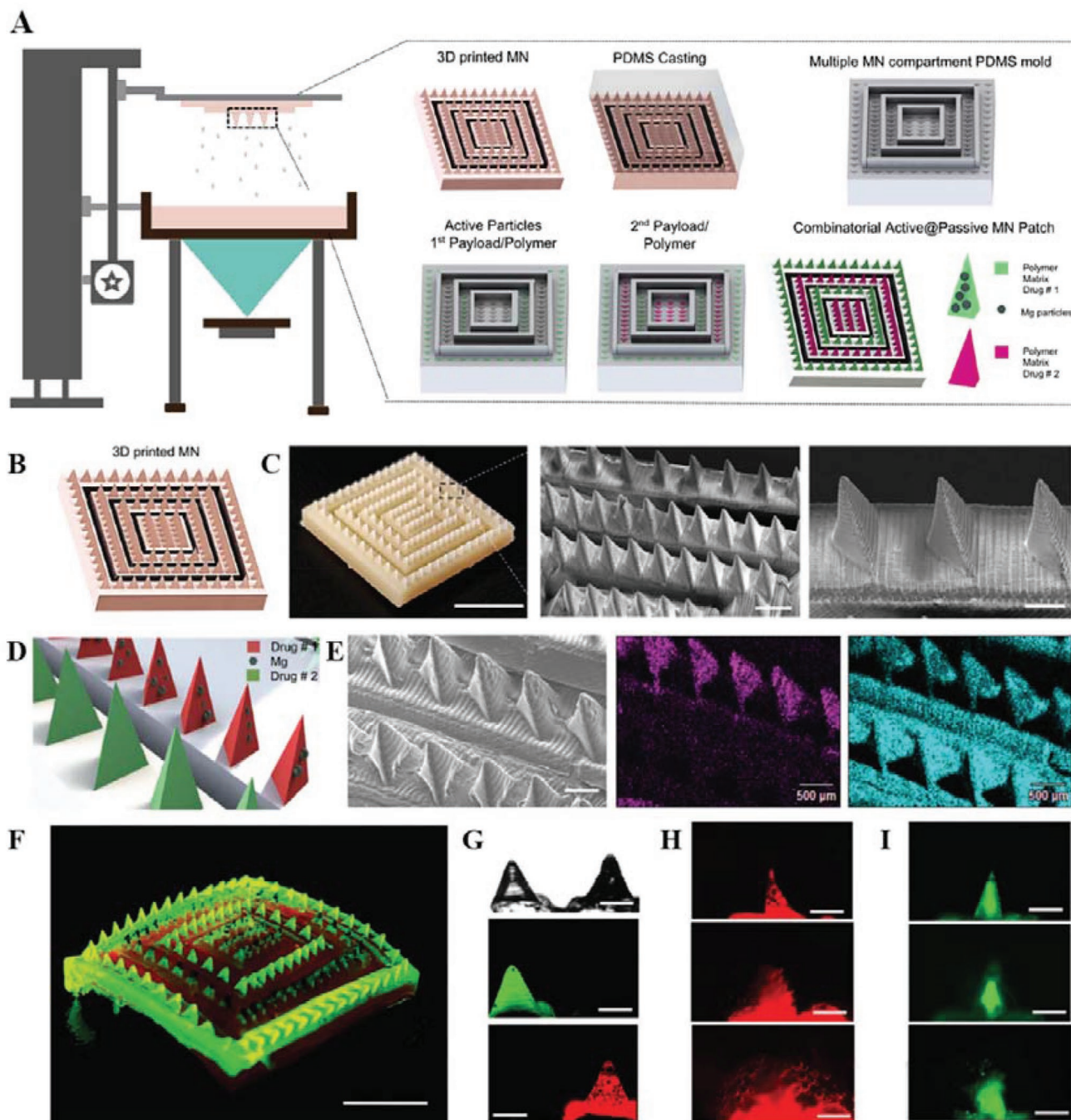


Figure 7. A) 3D printing and fabrication steps of polymeric combinatorial MN patch with spatially resolved active and passive MN zones. B) Schematic of square MN arrays as different active and passive compartments. C) Digital photograph of a 3D printed MN array by SLA and SEM images of MNs. Scale bars, 5 mm, 1 mm, and 500 μm respectively. D) Schematic of a combinatorial dissolvable MN patch with active and passive MN compartments. E) Side-by-side SEM image of active and passive MNs along with the corresponding EDX images illustrating the Mg in magenta, and C in cyan. F) Digital photograph of a combinatorial dissolvable MN showing active and passive MNs. Scale bars, 500 μm . G) Fluorescence patch loaded with FITC (passive MNs) and Rh6G + Mg particles (active MNs). Scale bar, 5 mm. H) Side-by-side optical and fluorescence microscopy images time-lapse images show the dissolution of an active MN tip at 10 s intervals. Scale bars, 500 μm . I) Fluorescence time-lapse images showing the dissolution of a passive MN tip. Scale bars, 500 μm . Reproduced with permission.^[108] Copyright 2020, Wiley.

inner diameter, 5 μm tip wall thickness) alongside a drug reservoir ($2 \times 1 \times 1 \text{ mm}^3$) were all fabricated from IP-S photoresist. Approximately half of the needle length penetrated into the

skin regardless of needle length. If the dimensions of MNs and spacing between needles were similar, the higher number of needles in the MN array led to the higher flow rate when

Table 3. Toxicological information of photoinitiators, photopolymers and UV curing agent-photoinitiator. Adapted from^[155] (N/A: not available).

Function	Compound or Trade name	Concentration [w/w]	Manufacturer	Toxicological information
Photoinitiator	Phosphine oxide compounds (Type II) including diphenyl(2,4,6-trimethylbenzoyl)-phosphine oxide (TPO) and bis acyl phosphine oxide (BAPO)	0.1–5%	Formlabs Dental and E-Shell series	LD ₅₀ Oral rat - > 5000 mg kg ⁻¹ LC ₅₀ (48 h) <i>Oryzias latipes</i> - 6.53 mg L ⁻¹
	Hydroxy-acetophenone (Type II)	N/A	N/A	LD ₅₀ Oral Rat - 2.240 mg kg ⁻¹ LC ₅₀ (96 h) <i>Salmo gairdneri</i> - 25 mg L ⁻¹
	Benzophenone compounds (Type II) including benzophenone-3 (BP-3) and benzophenone-4 (BP-4)	<10%	UV-cured inks	LC ₅₀ (96 h) <i>Pimephales promelas</i> - 14.2 mg L ⁻¹ BP-3 and BP-4: LC ₅₀ (48 h) <i>Daphnia magna</i> - 1.09 and 47.47 mg L ⁻¹
	1-hydroxy cyclo hexyl phenyl ketone (Irgacure 184)	N/A	Formlabs CIBA-GEIGY CORP	LC ₅₀ (96 h) <i>Danio rerio</i> - 24 mg L ⁻¹
Photopolymer	Acrylate monomers, acrylate and urethane acrylate oligomers	5–60%	Formlabs Autodesk Envision Tec	LD ₅₀ Oral rat - > 5000 mg kg ⁻¹ LC ₅₀ (96 h) <i>Cyprinus carpio</i> - 1.2 mg L ⁻¹ LC ₅₀ (96 h) <i>Pimephales promelas</i> - 34.7 mg L ⁻¹
	Methyl methacrylate monomers and oligomers	5–90%	Formlabs Envision Tec Dental resin	LC ₅₀ (96 h) <i>Cyprinodon variegatus</i> - 1.1 mg L ⁻¹ LC ₅₀ (96 h) <i>Lepomis macrochirus</i> - 283 mg L ⁻¹ LD ₅₀ oral rat - 7900 mg kg ⁻¹
	Tripropylene glycoldiacrylate	N/A	3D Systems	LD ₅₀ oral rat - 6800 mg kg ⁻¹ LC ₅₀ (96 h) <i>Leuciscus idus</i> - > 4.6–10 mg L ⁻¹
	3,4-Epoxy-cyclohexylmethyl 3,4-epoxy-cyclohexanecarboxylate	25–60%	3D Systems	LC ₅₀ (96 h) <i>Oncorhynchus mykiss</i> - 24 mg L ⁻¹ LC ₅₀ oral rats - 5000 mg kg ⁻¹
	1,6-bis(2,3-epoxypropoxy)hexane	15–30%	3D Systems	LC ₅₀ (96 h) <i>Leuciscus idus</i> - 30 mg L ⁻¹ LD ₅₀ oral rats - 2190 mg kg ⁻¹
	Tetraacrylate	30–60%	Formlabs Autodesk Envision Tec	LC ₅₀ (96 h) <i>Cyprinus carp</i> - 1.2 mg L ⁻¹ LC ₅₀ (96 h) <i>Danio rerio</i> - 7.9 mg L ⁻¹
	IP-S photoresist	N/A	Nanoscribe	LD ₅₀ oral - 500 mg kg ⁻¹
	IP-Dip photoresist	N/A	Nanoscribe	LD ₅₀ oral rat - 1830 mg kg ⁻¹ LD ₅₀ dermal rabbit - 4000 mg kg ⁻¹
UV curing agent and photoinitiator	Irgacure369	N/A	CIBA-GEIGY CORP	LD ₅₀ oral rat - > 5000 mg kg ⁻¹

compared to the array with less MNs. In addition, flow rate was reduced when the bore radius was decreased, and the shaft length was increased.

Like SLA 3D printing, TPP has been used in conjunction with micromolding, pulsed laser deposition and iron sputtering deposition to promote MN fabrication and functionalization.

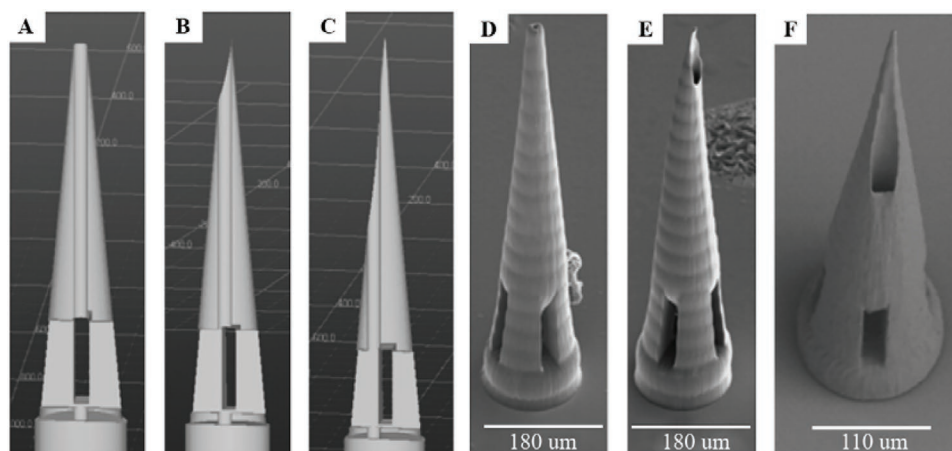


Figure 8. Computer-aided design diagrams of MNs with A) 0 mm, B) 1.4 mm, and C) 20.4 mm pore-needle center displacement values. SEM images of Ormocers MNs with D) 0 mm, E) 1.4 mm, and F) 20.4 mm pore-needle center displacement values. Adapted with permission^[10] Copyright 2007, The American Ceramic Society.

Gittard et al. developed polymeric MNs for insulin delivery using TPP and micromolding methods.^[111] The master MN, constituted of polyethylene glycol 200 diacrylate and Irgacure 369 photoinitiator, was fabricated using TPP into the following MN geometry; needle height 500 μm , needle base diameter 150 μm , and needle center-to-needle center distance 500 μm . Irgacure is a registered trademark of Advanced Biomatrix Inc, Carlsbad, USA. PDMS negative molds were subsequently produced using the master MN array as a template. A solution of eShell 200, a photo-reactive acrylate-based polymer, was subsequently casted onto the PDMS molds to form MNs. The eShell 200 MNs were capable of penetrating the SC of human skin, showing the feasibility in the delivery of insulin to enhance the patient compliance and increase the efficacy of active substances. In another study from Gittard et al., TPP-micromolding techniques were carried out to fabricate MN with antibacterial properties.^[113] Based on the same procedures from their previous study, polyethylene glycol 600 diacrylate MN containing gentamicin sulfate at the concentration of 2 mg/mL were obtained after casting drug-polymer solution on the PDMS molds that occupied the pattern of TPP-printed MNs. The geometries of such MNs were 500 μm in length with 150 μm base diameter, >10 μm tip diameter, and 45° tip angle. The growth of *Staphylococcus aureus* was visually inhibited in the presence of gentamicin sulfate-doped MNs in the agar plating assay.

Cordeiro et al. fabricated several highly detailed MN templates using TPP.^[158] Using such templates, reusable MN molds were reproducibly fabricated. These MN molds were subsequently used to produce dissolving and hydrogel-forming MNs. A flexible fabrication method, as a result of the synergistic combination of design and printing optimization, paved the way for producing high quality and mechanically strong master templates within a short period of time. Upon MN fabrication, promising results were obtained in terms of drug loading into dissolving MNs, insertion efficiency of MNs into skin stimulant, Parafilm M and in vitro drug permeation using hydrogel-forming MNs. Parafilm M is a registered trademark of Bemis Company, Inc, Wisconsin, USA. The flexibility and simplicity of this template fabrication method were key to facilitate the study of the impact of different MN array design parameters in the final performance of MN arrays as drug delivery systems.

Kavalzhiev et al. exploited TPP to fabricate a MN array, using iron coating technology or so-called sputtering deposition, to coat iron on the surface of the MN array, resulting in magnetic MNs.^[114] The magnetic properties of these MNs can be beneficial for biofunctionalization and visualization. To prepare a MN array, cylindrical, pyramidal, and conical MNs were fabricated based on dip-in laser lithography configuration and the crosslinking of IP-DIP liquid photoresist (Nanoscribe) occurred only in the focal spot controlled by TPP. After printing, the outer surface of the needles was coated with a homogeneous layer of iron using the sputtering deposition technique. As the size of cylindrical magnetic MNs (630 \pm 15 nm in diameter) was relatively smaller than the size of HCT 116 colorectal carcinoma cells (15.4 μm in diameter), a single MN could be used to penetrate the cell body and facilitate the intracellular delivery with no harm to the cell.

The temporary formation of pores on the SC created by MNs could cause skin infections by microorganisms.^[159] Gittard et al. combined TPP, micromolding and pulsed laser deposition to produce silver-coated MNs for preventing microbial infection after skin insertion.^[112] The master MNs were initially fabricated from the mixture of SR 259 polyethylene glycol dimethacrylate and Irgacure369 initiator by TPP, possessing 200 μm base diameter, 500 μm length, and 500 μm center-to-center interspacing. Using the micromolding technique with heat, Sylgard 184 silicone elastomer negative molds containing the shape of the master MN array were obtained. Sylgard is a registered trademark of Dow Inc, Michigan, USA. Subsequently, Ormocer-based MN were fabricated out of the molds and a thin film of silver was deposited on their surfaces by pulsed laser deposition. The silver-coated MNs exhibited non-cytotoxic effects to human epidermal keratinocytes and could effectively inhibit the growth of *Staphylococcus aureus*, a common bacteria causing the skin infection.

The performance of TPP in the production of complex MN structures is somewhat remarkable due to its high resolution. For instance, TPP has been demonstrated to successfully produce hollow MNs while other printing approaches (e.g., FDM) failed. Since TPP is capable of crafting a device in small scales, there have been reports on using TPP to combine MN arrays with microfluidic units (vide infra). In addition, TPP can be used in conjunction with micromolding to produce MNs in a mass production scale. However, in this regard, it is worth noting that SLA can offer the same benefit with a compromised resolution, but in a faster manner. Although one of the main advantages of TPP is printing resolution, it does have limitations, such as the shrinkage of the cured resin after photopolymerization as observed in other vat photopolymerization printing methods. This can potentially result in structural defects of the end product.^[160] Although many types of resin used in TPP are compatible with skin cells, there is a lack of human studies to determine any possible adverse effects of the resins. In conclusion, even though TPP can achieve high precision printing, there are also several factors to consider prior to adopting this technology for MN production. For example, its long processing time, cost of production, requirement of photo-sensitive resins, and structural integrity of the objects.

3.2.3. Continuous Liquid Interface Production (CLIP)

Modified from SLA, CLIP replaces a UV transparent window with an oxygen permeable window.^[47] CLIP proceeds via projecting a continuous sequence of UV images (generated by a digital light-processing imaging unit) through an oxygen-permeable, UV-transparent window below a liquid resin bath.^[161] This oxygen permeable window creates a dead zone, a thin uncured liquid layer between the window and the cured part surface, which prevents the resin from curing and attaching to the window.^[47] Unlike SLA, the fabrication of objects using CLIP is no longer in a layer-by-layer manner but instead the production occurs continuously and rapidly as the separation and realignment steps are removed.^[161] The objects produced by CLIP therefore have a smooth surface with no stacking artifacts observed.

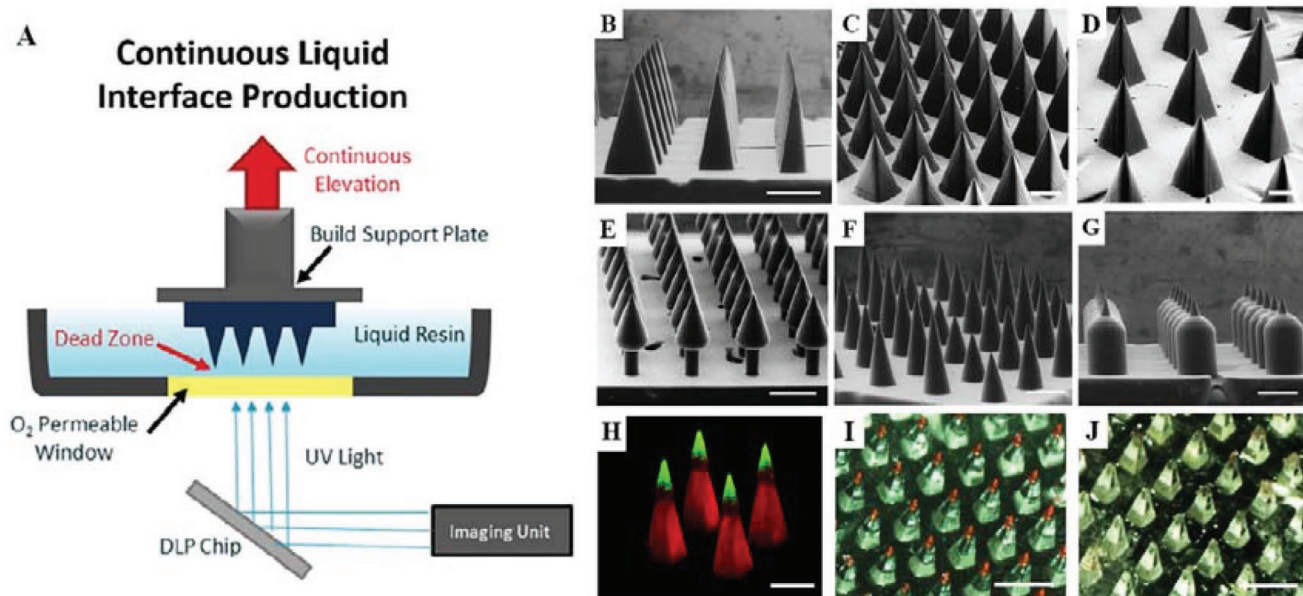


Figure 9. A) Continuous Liquid Interface Production (CLIP) process. B–D) TMPTA MNs of aspect ratio 2, 3, and 4, respectively. E) Arrowhead MNs. F) Tiered MNs and G) turret MNs. H) Confocal micrograph of a Janus MN, where the MN base is composed of polycaprolactone encapsulating rhodamine (red) and the MN tip is composed of polyacrylic acid encapsulating fluorescein (green). I) Janus MNs with a water-soluble rhodamine containing tip before application to murine skin and J) Janus MNs after application to murine skin. Scale bars are 500 μm for all images except those for I and J which are 1 mm. Adapted with permission.^[47] Copyright 2016, PLOS.

Johnson et al. has shown the feasibility of CLIP to rapidly fabricate MNs from various polymers in different geometries and shapes including pyramidal, arrowhead, tiered, and turret MNs (Figure 9).^[47] Within 90 s, the array of MNs was produced with high accuracy. The MNs fabricated by CLIP in this study could penetrate the skin and rapidly deliver rhodamine B, which was encapsulated in MNs, into ex vivo murine skin. The benefit of CLIP is that it is not limited to the production of MNs from a single material. Johnson et al. demonstrated that by simply changing the resin in the vat at the predetermined printing time, the MNs could be produced with a rhodamine B-loaded PCL basement and a fluorescein-loaded acrylic acid tip. This potentially promotes the development of polydrug-loaded MNs.

3.2.4. Microstereolithography

Microstereolithography is a high-resolution, rapid prototyping method capable of producing 3D microstructures with greater precision than SLA. The principle of microstereolithography is classified into three categories: scanning, projection and sub-micrometer resolution. Herein, only projection-based microstereolithography will be described as it is the only approach used for MN fabrication to date. Similar to SLA, fabrication of prototypes is based on the polymerization of resin but instead of using UV light to scan the vat point-by-point, projection-based microstereolithography illuminates a digital image of each 2D slice to cure the resin immediately. A series of 2D slices is used to generate sequential dynamic mask patterns for the projection of micro-sized laser beam on the resin surface, controlled by a digital micromirror device. Consequently, the UV curable

resin solidifies into shape where it is exposed to the light. After the first layer is completely fabricated, the printed structure is immersed into the resin vat to allow the fabrication of a new layer on top of the former. It should be noted that projection-based microstereolithography is also referred to as direct light projection (DLP) 3D printing technology.

Fabrication of MNs with different geometries using microstereolithography was first introduced by Choi et al. to study the effect of geometry on needle insertion and fracture force.^[118] Three different MNs were designed to consist of two parts, a quadrangular pyramid and a square pillar, in various ratios (1:1, 2:1, and 1:2) as shown in Figure 10. The dimensions of all MNs were kept constant at 900 μm height, 200 μm base, and 20 μm tip. In order to puncture the skin without breaking, MNs should have a fracture force higher than the insertion force. Sharp needle tips can reduce the insertion force and increase the fracture force as the stress is concentrated at the smallest cross-sectional area, which is the needle tip. Consequently, in this study, the MNs with the ratio of 1 quadrangular pyramid to 2 square pillars showed the best resistance against the load.

After this, researchers began fabricating MNs or MN master templates by microstereolithography using a biocompatible, commercially available acrylate-based polymer known as eShell, which is used in fabrication of thin-walled hearing aid shells. Firstly, Gittard et al. fabricated eShell 200 MNs by visible light dynamic mask microstereolithography, using pulsed laser deposition to coat a thin film of silver or zinc oxide on the surface of MNs.^[119] Silver and zinc oxide coated MNs exhibited anti-bacterial properties against *Staphylococcus epidermidis* and *Staphylococcus aureus*, two common gram-positive bacteria causing skin infections, in the agar diffusion assay. The MNs were able to insert the porcine skin, promote wound healing by

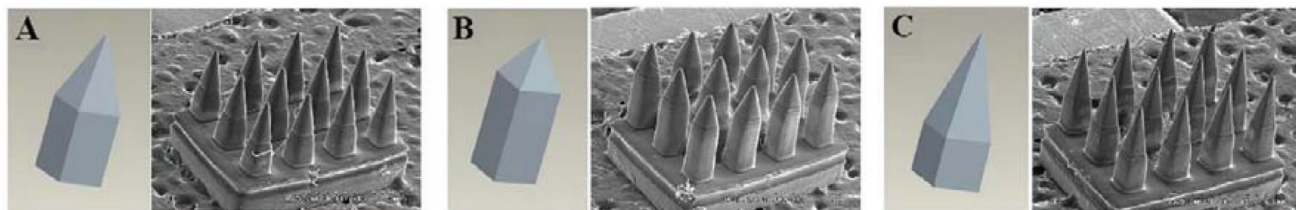


Figure 10. Model and MNs fabricated by microstereolithography with the ratio of quadrangular pyramid and square pillar as A) 1:1; B) 1:2 and C) 2:1. Adapted with permission.^[118] Copyright 2006, IEEE.

holding the skin around the wound area together and inhibit the growth of bacteria at the application site. Second, Boehm et al. introduced a scalable and low-cost approach for producing quantum dot-coated MNs based on three technologies; visible light dynamic mask microstereolithography, micromolding and piezoelectric inkjet printing.^[122] A master MN mold was fabricated out of eShell 200 by microstereolithography and subsequently used as a template for PDMS mold production by micromolding method. Gantrez AN-139 MNs with cylindrical base and conical shaped tip were produced from such PDMS molds and the outer surface of MNs was later coated with quantum dots by piezoelectric inkjet printing. The surface coating by piezoelectric inkjet printing was highly reproducible, offered minimal contamination, and could be performed at room temperature. The Gantrez AN-139 MNs created temporary pores on the porcine skin, enabling the delivery of quantum dots into the skin with a penetration depth greater than 200 μm . Following on from this, Boehm et al. fabricated pyramidal-like MNs from Gantrez AN 169 BF for skin infection treatment (**Figure 11**).^[50] The MNs coated with Qtracker 705 non-targeted quantum dot solution by inkjet printing exhibited anti-bacterial properties against the growth of *Escherichia coli*, *Staphylococcus aureus*, *Enterococcus faecalis*, and *Bacillus subtilis* in agar plating test after 24 h incubation. Qtracker is a registered trademark of Life technologies, New York, USA.

Yun and Kim showed the use of projection-based microstereolithography in the fabrication of multimaterial MNs.^[120] The MN base was manufactured from general resin, while the body of MNs was constituted of biodegradable poly(propylene fumarate). These MNs were designed to release drug encapsulated in the MN body at a fixed rate. Lu et al. utilized digital micro-mirror device-based microstereolithography to produce dacarbazine-loaded poly(propylene fumarate)/diethyl fumarate MNs

for the potential treatment of skin cancer.^[121] Dacarbazine was uniformly blended into the poly(propylene fumarate)/diethyl fumarate solution prior to crosslinking. The MNs were conical-shaped (700 μm height, 200 μm width) with a conical tip of 300 μm height and 20 μm tip radius. Following in vitro release kinetic studies, a burst release of dacarbazine from the MNs was observed in the first week, followed by a sustained release over a 5 week period. These results highlighted the ability of microstereolithography to be used as a suitable technique to fabricate drug-loaded MNs.

Lim et al. interestingly fabricated personalized MN splints targeting joint inflammation in trigger finger disease (**Figure 12**).^[116] Initially, the finger was “patched” with a liquid formulation of diclofenac diethylamine. Subsequently, a MN splint containing solid MNs was applied to the finger to perforate the SC for transdermal drug delivery. MNs in the splint were fabricated from resin. The MN height was 900 μm , base diameter was 300 μm , and the center-to-center spacing between each needle was 1800 μm . Significantly higher permeation of diclofenac diethylamine (ca. fivefolds, p -value < 0.01) was observed in the skin treated with the MN splint when compared to topically applied diclofenac diethylamine only.

More recently, Yao et al. prepared MNs from a mixture of polyethylene glycol diacrylate (PEG400DA) monomer and phenylbis(2,4,6-trimethylbenzoyl)phosphine oxide.^[117] By varying the light exposure time, mechanical properties of MNs changed accordingly. The stiffness of MNs was increased when the exposure time was longer. Additionally, Yao et al. observed that the DLP fabricated MNs contained many micro-pores, which promoted the transdermal delivery of rhodamine B into the skin and also facilitated the extraction of rhodamine B from the artificial skin within 30 min.

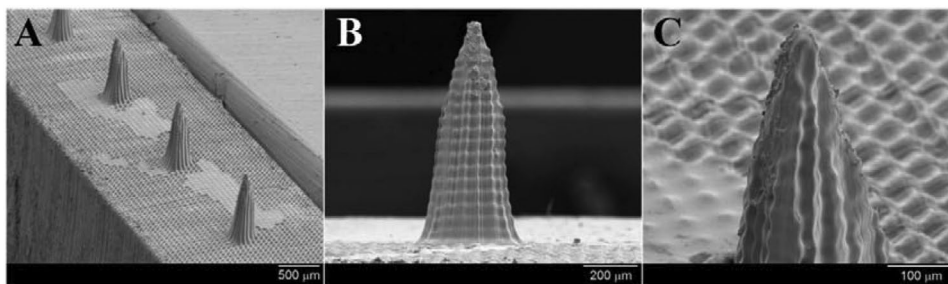


Figure 11. SEM images of Gantrez AN 169 BF MNs within a five-MN array produced by visible light dynamic mask microstereolithography micromolding. A) Three Gantrez AN 169 BF MNs; B) An individual Gantrez AN 169 BF polymer MN and C) the tip of an individual Gantrez AN 169 BF polymer MN. Reproduced with permission.^[50] Copyright 2012, IOP Publishing.

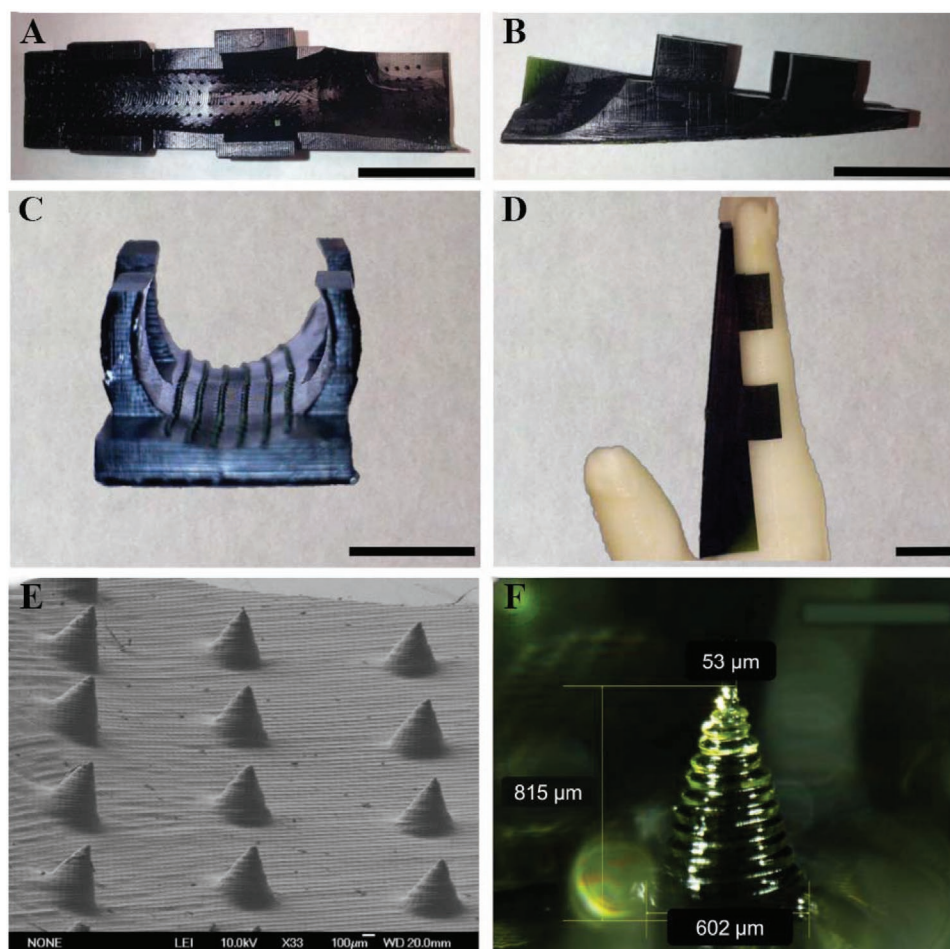


Figure 12. Images of the MN splint. A) top view of the splint (scale bar = 2 cm); B) side view of the splint (scale bar = 2 cm); C) top view of the arrays of MN 3D printed on the inner surface of the splint (scale bar = 1 cm); D) side view of the splint fitted onto the hand model (scale bar = 1 cm); E) SEM image of MNs on a personalized contoured surface of the splint and F) a single MN on personalized contoured surface. Reproduced with permission.^[116] Copyright 2020, Wiley.

3.3. Powder Bed Fusion

3.3.1. Selective Laser Melting (SLM)

Selective laser sintering (SLS) 3D printers are based on a laser beam, which acts as a concentrated heating beam to sinter tightly thermoplastic powders. Sintering refers to the process of heating powder particles so that they stick together to form a solid structure without reaching the melting point of the powder. SLM 3D printing uses a similar technique to SLS, but in this 3D printing method, sintering is taken a step further and a laser is used to achieve a full melt of the materials used.^[162] SLM has been used to fabricate hollow MNs. For the first time, Gieseke et al. developed a micro SLM system to produce biocompatible hollow MNs from stainless steel alloy 316L powders (Figure 13).^[123] Complex structures were fabricated by using a small laser spot diameter (19.4 μm) and fine particles (5–25 μm). The MNs fabricated by this method had a grainy surface due to non-uniform powder spreading. Moreover, some parts of hollow MNs were blocked because of high energy input-induced powder adherence along the wall. Although

it is recognized that the depositing mechanism needs to be improved in order to enable a smoother MN finish, this study highlighted the huge potential of fabricating hollow MNs using a SLM 3D printer.

SLM is a powder bed-based layer-by-layer fabrication method with high resolution.^[163] One of the advantages of SLM printing is that various materials can be used and their properties can be easily tuned during manufacturing. In addition, the costs associated with this method are budget effective.^[164] On the contrary, the materials used in powder-based printing methods include metallic alloys (e.g., stainless steel, nickel, aluminum, and titanium). The biocompatibility of these metals therefore needs to be considered. Moreover, the end product of the SLM method is formed by laser-guided powder melting. This can cause a microscopic anisotropy of material along the building direction, hence brittle products are obtained. Due to the use of powders as the raw material, as previously discussed, MNs fabricated by SLM possess undesired rough surfaces. As a result, an extra polishing step is required. Generally, the surface roughness of SLM printed parts can be improved by different post-processing approaches. This includes sand blasting,

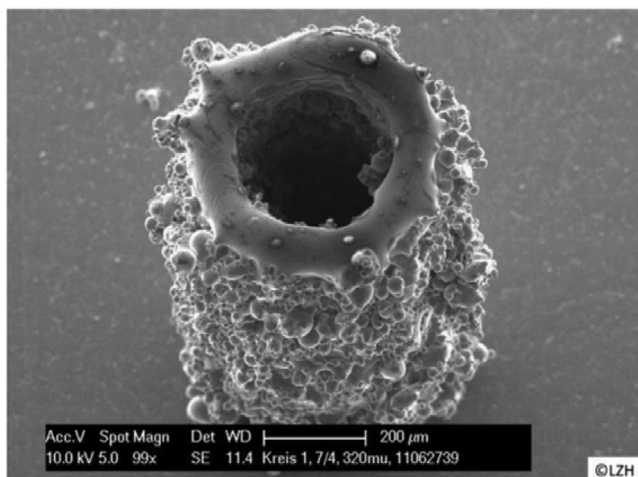


Figure 13. SEM image of hollow MN produced by micro SLM. Reproduced with permission.^[123] Copyright 2012, De Gruyter.

shoot peening, electropolishing, chemical polishing, grinding, machining, vibratory finishing, and drag finishing.^[165,166] However, it is worth noting that these approaches require a skilled operator and are difficult to apply uniformly on complex-shaped parts. As a consequence, it is challenging to improve the surface roughness of MNs produced by the SLM method due to complexity and miniscule sizes of the MN structure.

Shortly after the advent of 3D printing technology, it has become popular in the field of drug delivery as a tool for MN production. Various 3D printing techniques have shown that they can manufacture MNs in different manners, such as different sizes, shapes, and features. Each technique offers different benefits in MN fabrications. For example, SLA and TPP can provide a well-controlled geometry of MNs. However, it also inevitably comes with some caveats, such as long production time and an unsmooth surface of the finished objects. The current development on 3D printing techniques aims to eliminate those limitations while attempting to achieve better outcomes, such as strong and sharp MNs. Standing out from other 3D printing methods, CLIP offers shorter processing times, smoother surface of MN, and more flexibility in MN geometry. It is believed that this method will become the future of MN production, particularly in the field of drug delivery. Meanwhile, microstereolithography also provides higher precision and faster production than SLA. Nevertheless, the undesired stacking effect which causes uneven edges of the objects is always observed due to the nature of layer-by-layer fabrication. However, the MNs manufactured by this method often possess decent mechanical strength and sharpness. Moreover, post coating of the MNs with drugs can be done for transdermal drug delivery. SLM is the method that allows powder materials to be used as a printing material. However, the produced MN has rough surfaces, which can badly affect their performance on skin insertion. Additionally, the mechanical strength of MN tends to be too low due to the anisotropic property after printing. The tips of the MN may snap and remain in the skin. The safety aspect should be carefully considered if the fabrication of MN is based on this method.

Considering that the height of MNs is typically less than 2000 μm to avoid pain receptor stimulation, the printers

available on the market with Z-axis resolution in the range of 10 nm to 10 μm are the most promising tool to produce sharp MNs with heights below 2000 μm . This is because the printers with a higher resolution can slice a CAD design of MNs into more and thinner layers compared to those with a lower resolution. As a result, much finer detail of MNs can be achieved, especially the tip section, which significantly impacts the insertion ability. Römgens et al. investigated penetration depth into ex vivo human skin of single solid MNs with different tip diameters (5, 15, 24, and 37 μm) and force required by these MNs for skin insertion.^[167] It was observed that the MNs with 5 μm tip diameter could insert into the skin deeper and required less force for the skin insertion when compared to the MNs with larger tip diameters (20 mN for 5 μm tip diameter and 167 mN for 37 μm tip diameter). Khanna et al. also showed that increasing the sharpness of hollow silicon MNs resulted in lower insertion force required to insert the MNs into human cadaver skin (10.97 gf for 119.8 μm tip diameter and 475.14 gf for 153.9 μm tip diameter).^[168]

Table 4 shows the Z-axis resolution, accuracy, speed, and relevant costs of 3D printing methods. Except for FDM, most 3D printing methods possess good resolution and accuracy for printing MNs. This is in accordance with several precedent studies that FDM printers cannot independently produce intricate MNs. Hence, additional steps or techniques are required to refine MN shapes, such as chemical etching.

4. 4D Printing

While 3D printing becomes more popular, the term, 4D printing is a new and emerging printing technique.^[175] 4D printing enables a printed structure to change its form or function with time following external stimulation such as pressure, temperature, wind, water, or light.^[176] Therefore, this new dimension provides great potential to further widen the application areas of 3D printing.

Interestingly, MNs have been recently manufactured using 4D printing. In a study by Han et al. (2020), MNs containing backward-facing barbs were fabricated using 4D printing in order to increase MN adhesion to the skin.^[49] In this study, to achieve the concept of 4D printing, projection-based microstereolithography was used in conjunction with a programmed shape deformation of barbs employing printing process-induced crosslinking density gradient (**Figure 14**). MNs were fabricated from poly(ethylene glycol) diacrylate (PEGDA 250), phenylbis(2,4,6-trimethylbenzoyl)phosphine oxide, and Sudan I that served as a monomer, photoinitiator (PI), and photoabsorber (PA), respectively. While PI concentrations controlled the reactivity of the precursor, the PA played a critical role in the penetration depth of light. The thickness of barbs increased with longer light exposure time, higher PI concentrations and lower PA concentrations. Also, since the light irradiation intensity reduced while traveling through the precursor solution, this resulted in gradient crosslinking density through the layers. The upper layers were relatively more crosslinked than the lower layers. Some uncrosslinked monomers in the lower layers could be removed by immersing the MN in ethanol (desolvation), hence void areas beneath the barbs were generated. Upon drying, the barbs

Table 4. Information of Z-axis resolution, accuracy, speed, and relevant costs of different 3D printing methods^[149,161,169–174] (N/A: not available).

Method	Z-axis resolution [μm]	Accuracy [μm]	Speed	Equipment costs ^{a)}	Material costs ^{a)}	Labor needs/production time
FDM	50–2000	100	N/A	\$199–\$185 000 Budget printers start from few hundred dollars. Higher quality mid-range desktop printers start from \$2000. Industrial systems start from \$15 000.	\$15–\$180 per kg for filaments \$100–200 per kg for support materials	Manual support removal Lengthy postprocessing is required for a high-quality finish.
SLA	10–200	0.5–50	N/A	\$170–\$490 000 Professional desktop printers start from \$3500. Large-format benchtop printers start from \$11 000. Large-scale industrial machines start from \$80 000.	\$50–\$250 L ⁻¹ for resins	Washing and postcuring Simple postprocessing to remove support marks
TPP	0.08–0.15	0.5–50	100 μm s ⁻¹	\$350 000+	N/A	Processing time > 3 h for MN arrays
CLIP	50–100	0.5–50	1–5 μm min ⁻¹	\$64 000–\$162 500	\$99–\$399 per L for resins	Washing and post-curing
Microstereolithography	0.6–200	10–62	60 mm h ⁻¹	\$450–\$250 000	\$50–\$435 per L for resins	Washing and postcuring Postprocessing to remove any support and to polish the printed part
SLM	20–500	N/A	N/A	\$250 000–\$500 000	\$5 per kg for aluminum \$50 per kg for nickel \$75 per kg for steel \$150 per kg for titanium	Postprocessing to improve surface quality Part separation can take from an hour up to 2 d

^{a)}Estimated equipment and material costs are from the website of manufacturers and suppliers, latest updated in January 2022.

shrunk and bended downward. The MNs with barbs improved the skin adherence and displayed an 18-fold increase in mechanical strength when compared to MNs without barbs. Additionally, the MNs with barb structures could carry a high quantity of drug, promoting drug delivery through the skin.

5. Integration of 3D Printing with Other Technologies to Develop and Produce Novel MNs

The diversity and versatility of operations enabled by 3D printing can be segmented through the integration of other technologies to fabricate MNs. In this section, examples of conjunct technologies, such as microfluidics, electrodes, and cell encapsulation in combination with 3D printing are described. **Table 5** summarizes the examples of MNs fabricated by 3D printing methods combined with conjunct technologies.

5.1. Integration of 3D Printing with Microfluidic Technology

Microfluidic is a technology designed to manipulate a minuscule amount of fluids that are confined in a network of microscopic

channels, which are embedded in a small device.^[182,183] The miniaturization of microfluidic technology offers several advantages. The key benefit is that the manipulation of such a device requires a small volume of fluid (picoliter to nanoliter).^[183,184] The ease of use and low production cost make microfluidic technology very attractive. Other advantages include high analytical throughput, high sensitivity and specificity, facile parallelization through multiplexing, and minimal contamination.^[184–186] Microfluidic devices can be fabricated from several methods (e.g., laminate, photolithography, soft lithography, hot embossing, injection molding, laser ablation, and 3D printing) and materials (e.g., metal, glass, quartz, and polymers).^[183,186,187] In the past decade, the applications of microfluidic technology are widely expanding to the pharmaceutical field, medicine and biology, such as bioassays, drug screening and analysis, tissue engineering and medical diagnostics.^[182,184] Recently, the integration of microfluidic technology with a MN has gained a huge interest due to their similarity in size range. 3D printing has highlighted the possibility of merging both technologies together. This not only can reduce the cost of production, but it also adds new features to the device to facilitate more precise drug delivery or more effective interstitial fluid extraction. Although microfluidic devices have been reported to be

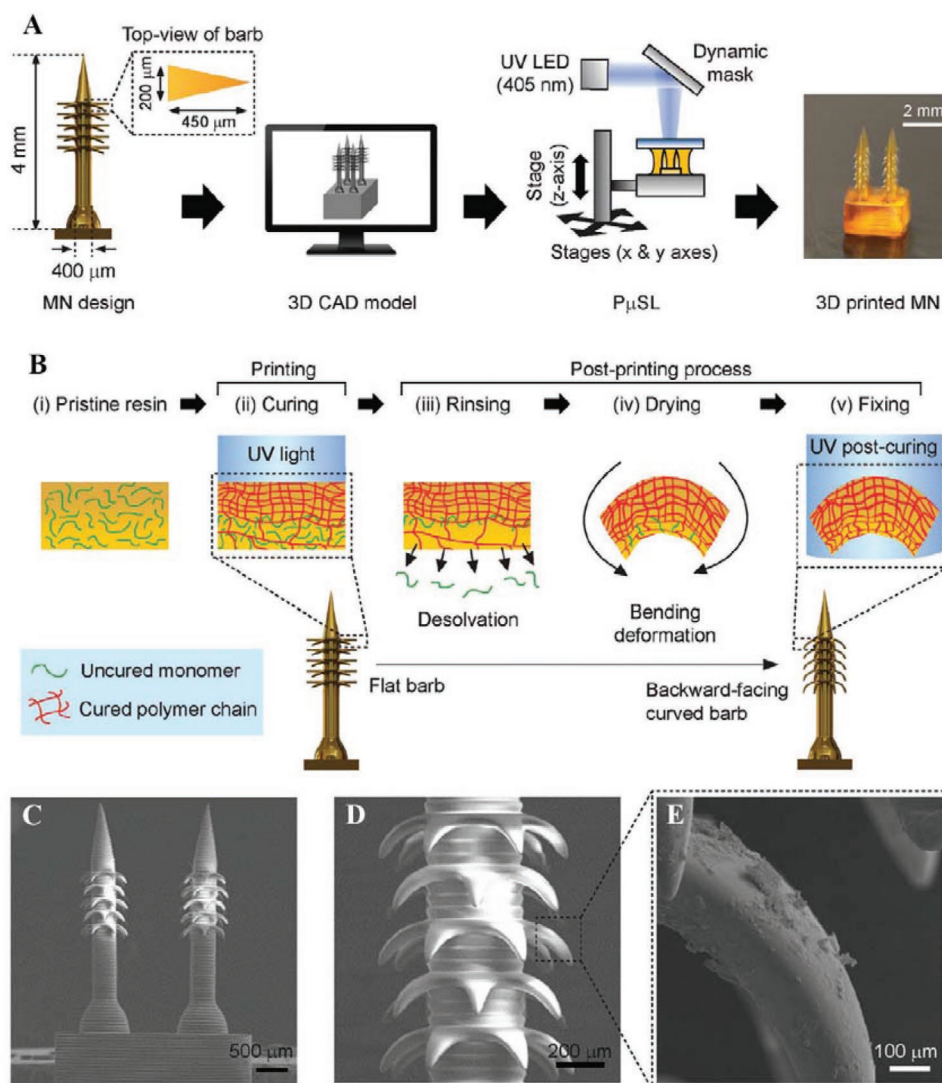


Figure 14. 4D printing of bioinspired MN using projection-based microstereolithography. A) Schematic illustration of the projection-based microstereolithography process. B) Schematic illustration of 4D printing approach to program deformation of horizontally printed barbs into a backward-facing shape. C–E) SEM images of 4D printed MN array with backward-facing barbs. Reproduced with permission.^[49] Copyright 2020, Wiley.

produced by FDM, only SLA and TPP are the preferred options for manufacturing microfluidic-MN devices. This is perhaps due to the low resolution of FDM, which leads to high surface roughness of the end product when compared to SLA and TPP.^[187] SLA-microfluidic and TPP-microfluidic technology will now be discussed in turn.

Yeung et al. demonstrated the use of SLA 3D printing to manufacture intricate microfluidic-enabled MN devices in a single step (Figure 15).^[46] Different geometries of hollow MNs resulted in different penetration depths. The printed geometries included two of the most commonly reported 3D printed MN designs: a pyramidal MN with a triangular base and tip orthogonally aligned with a vertex of the base and a conical MN with tapered sidewalls. With this, a fine-tip syringe-shaped MN design was also manufactured. Conducting insertion studies using Parafilm M, it was concluded that the syringe-shaped MN design maximized depth and ease of insertion compared to

other designs tested. Therefore, the syringe-shaped MN design was taken forward for further studies. An *ex vivo* transdermal drug delivery study was performed. In this work, this MN design was integrated with microfluidic modules. Model drug solutions, rhodamine B, fluorescein isothiocyanate, and methylene blue were injected through the device and into porcine skin. Homogeneous mixing of multiple fluids was achieved at various flow rates and *ex vivo* confocal laser scanning microscopy validated the device's ability to transdermally deliver these model drug solutions in a controlled manner.

Cylindrical-shaped hollow MN-open microfluidic channel devices integrating TPP, micromolding, soft embossing and microfluidic technology were produced by Rad et al. (Figure 16).^[178] Along the body of the MN, an open channel was aligned at the side from the tip to the base of the MN. This open channel was subsequently extended to a reservoir at the base of the MN. After preparing master templates using PDMS,

Table 5. Examples of MN embedded devices fabricated by 3D printing technology and other technologies.

Fabrication method	Conjunct technology	Material(s)	Geometry	Application(s)	Refs.
SLA	Microencapsulation	Resin	Hollow MNs	Cell delivery	Farias et al. ^[177]
TPP	Microfluidic	IP-S photoresist for master MNs; cyclo-olefin polymer for MNs	Cylindrical hollow MNs	Drug delivery and collection of subcutaneous fluid	Rad et al. ^[178]
TPP	Microfluidic	Resin	Hollow MNs	Drug delivery	Yeung et al. ^[146]
TPP	Microfluidic	OrmoComp	Hollow MNs	Drug delivery and fluid extraction	Trautmann et al. ^[179]
DLP	Carbon fiber electrode	eShell 200	Hollow MNs	Electrochemical sensor	Miller et al. ^[180]
Microstereolithography	Electrodes	eShell 300	Hollow MNs	Biosensor for pH, glucose and lactate detection	Miller et al. ^[181]

MNs were fabricated from thermoplastic pellets, cyclo-olefin polymer, Zeonor 1060R. Due to the hydrophobic nature of this polymer, oxygen plasma treatment was carried out to make the surface of MNs and open channels more hydrophilic. This step was conducted so that the MN could encourage passive filling of the open channels and reservoir of ISF from the skin in future experiments. After performing physical characterization tests on these novel MNs, the delivery of model drug, fluorescein was investigated. MNs were dip-coated into a concentrated

aqueous solution of fluorescein. The penetration of fluorescein into a rabbit ear was visualized by two-photon optical sectioning. This proof-of-concept study demonstrated the potential application of 3D MN prototyping, TPP, micromolding and embossing for drug delivery.

In another example, Trautmann et al. combined TPP with microfluidic technology to create hollow MNs connected with microfluidic channels for drug delivery and fluid extraction.^[179] These MNs were fabricated by TPP into conical and pyramidal

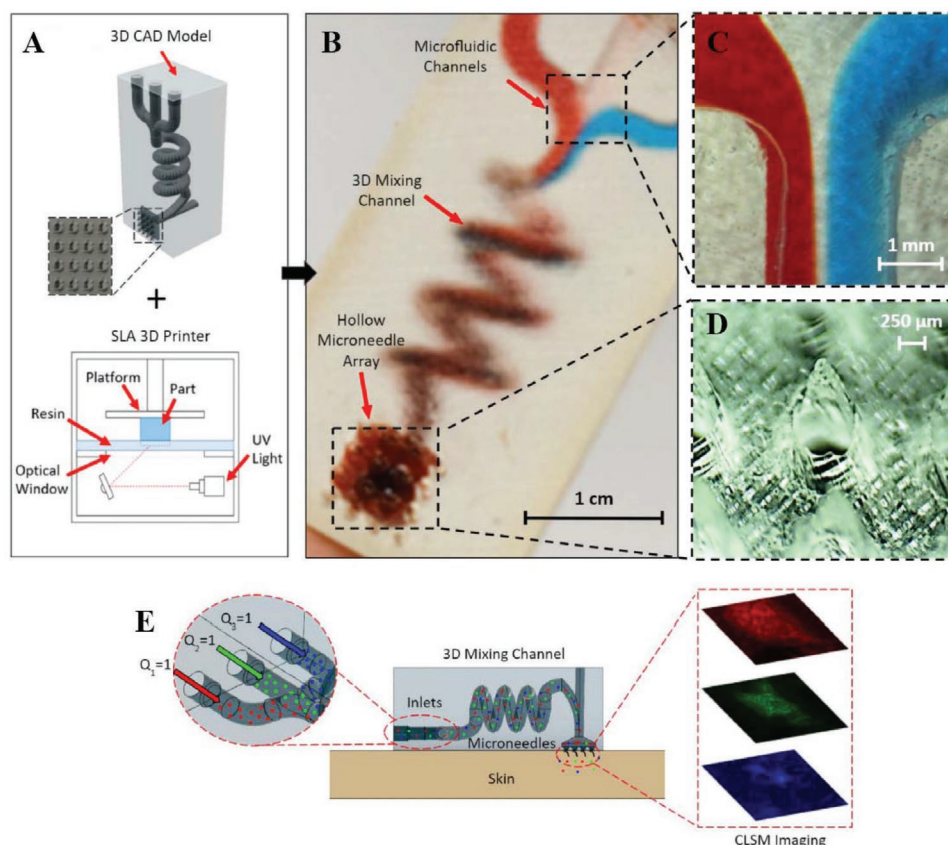


Figure 15. 3D printing of microfluidic-enabled hollow MN devices. A) CAD model of a representative microfluidic-enabled MN device as an input to the SLA printer. B) The printed device with three microfluidic inlets converging into a 3D spiral chamber and to a hollow MN array outlet. C) Close-up of the inlet junction visualizing the convergence of red-dyed, clear, and blue-dyed solution streams. D) Close-up of the hollow MN array and E) The schematic diagram of the experimental setup and the CLSM imaging area. Adapted with permission.^[146] Copyright 2019, AIP.

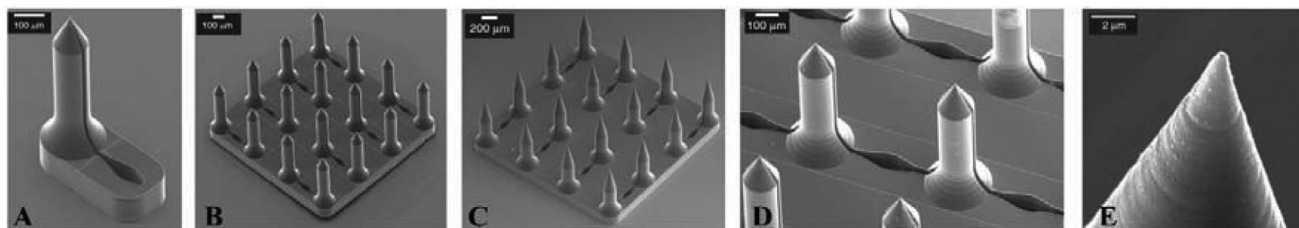


Figure 16. A) SEM image of fabricated single open-channel MN connected to a reservoir by 3D laser lithography. B) A MN array with side channels connected to reservoirs, MNs have 700 μm total height, 150 μm tip height, 150 μm flange height. C) A MN array with side channels connected to reservoirs, MNs have 700 μm total height, 350 μm tip height, 150 μm flange height. D) MNs having two side-opened channels connected to different reservoirs and E) Ultrasharp MN tip. Adapted with permission.^[178] Copyright 2107, Springer Nature.

shapes with a truncated tip, and subsequently connected to the microchannels which were generated in the internal polymethyl methacrylate bulk material by a femtosecond pulse laser system. Each MN geometry was further modified to have different wall angles which were 11° for thin MNs and 24° for thick MNs. Owing to the property of photosensitive material, OrmoComp, the MNs were mechanically strong enough to penetrate porcine skin and remained intact after several skin insertions. OrmoComp is a registered trademark of micro resist technology GmbH, Berlin, Germany. The functionality of MNs-microfluidic channels was demonstrated by running rhodamine B and distilled water through the structure. This study showed that both low viscous rhodamine B in distilled water solution ($\approx 1 \text{ mPa s}$ at 20 °C) and viscous ethylene glycol (20.81 mPa s at 20 °C) could run through an opening orifice of 30 μm and fill up the microchannels.

5.2. Integration of 3D Printing with Carbon Electrodes

To continuously monitor the level of metabolites (e.g., glucose, lactate, uric acid) in a non-invasive manner, many wearable biosensors have been extensively developed to detect biomarkers in saliva and sweat.^[188–190] Biosensors are devices that enable a real-time analysis of analytes in a biological sample.^[190] An electrode used in biosensors can be made of a variety of materials (e.g., silver, gold, nickel, platinum and carbon).^[191] The choice of material for making an electrode is dependent on the purpose of the sensor. Since carbon is inert, biologically compatible, cheap, electrical conductive and possesses a high surface area, it is most commonly used for making an electrode in electrochemical biosensors.^[191–194] Interestingly, 3D printing, particularly microstereolithography, has been used in combination with carbon electrodes to monitor analytes in situ. In this regard, two examples will now be discussed.

Firstly, Miller et al. fabricated tetrahedron-shaped hollow MNs out of eShell 200 using microstereolithography and manually inserted carbon electrodes into the inner structure of hollow MNs to generate a real-time electrochemical sensing device.^[180] These MNs exhibited biocompatibility to human dermal fibroblasts and neonatal human epidermal keratinocytes, and the integrity of these MNs remained intact after the removal from the skin. The carbon electrodes integrated within the hollow MNs also showed the ability to detect the presence of ascorbic acid and also hydrogen peroxide via palladium-catalyzed oxidation. Second, Miller et al. developed a MN-based

biosensor for multiplexed in situ detection of pH, glucose, and lactate.^[181] A hollow MN was fabricated out of eShell 300 acrylate-based polymer using projection-based microstereolithography. Subsequently, the MN was aligned on a flexible flat cable that contained a laser-ablated opening well filled with specially formulated carbon paste for pH, glucose, or lactate detection. The device was capable of selectively detecting changes in pH, glucose and lactate over physiologically relevant concentrations, offering the potential application for detecting metabolic acidosis and monitoring tumor microenvironment.

5.3. Integration of 3D Printing with Cell Microencapsulation

The microencapsulation of cells in a biocompatible matrix has gained a lot of interest in the fields of drug delivery and regenerative medicine. This technology involves the encapsulation of cells in a semipermeable membrane (commonly made of biocompatible polymer), which allows the exchange of nutrients, oxygen, waste, and therapeutic factors secreted by the entrapped cells.^[195,196] This semipermeable membrane also protects against the elimination of delivered cells by immune cells, antibodies and high molecular weight molecules. As a result, the rejection of graft is decreased and immunosuppressants are not required for transplantation.^[197] In the regard of regenerative medicine, cell microencapsulation can be used for the direct delivery of cells to the targeted wound area. These cells will subsequently promote the wound healing process by secreting cytokines and growth factors to induce the formation of new tissue. Regarding drug delivery, cell microencapsulation has been used in combination with the fabrication of MNs through 3D printing. For example, Farias et al. investigated the feasibility of using hollow MNs fabricated from biocompatible resin (FLGPCL02 photoresin) by SLA 3D printing as a platform to deliver human hepatocellular carcinoma (HepG2) cells encapsulated in crosslinked alginate capsules.^[177] FLGPCL02 photoresin is a registered trademark of Formlabs Inc, Massachusetts, USA. The device consisted of a cylindrical cell reservoir and MN in which the shape and tip radius of MNs were conical and $162.5 \mu\text{m} \pm 20 \mu\text{m}$, respectively. The device was not cytotoxic and the viability of HepG2 cells post-extrusion at 24 h from the device was not significantly different ($p = 0.500$) from nonextruded control cells. Hence, this could be considered as a new approach for cell delivery to enhance wound healing at a specific site.

6. Conclusion

3D printing technology shows promising feasibility in fast production of complex MN structures for drug delivery and skin fluid extraction. 3D printing methods which are based on light-induced polymerization can produce MNs in higher resolutions and with smoother surfaces when compared to hot-melt extrusion-based and powder bed-based 3D printing approaches. Various 3D printing methods enhance the performance of MNs in skin penetration by shape and geometry modification, facilitating the delivery of drug to the deeper layers of the skin. Emergence of 3D printing with conventional techniques such as hydrogel shrinkage and micromolding results in MNs with smaller sizes or finer features. Moreover, 3D printing integrated with other technologies can create customized drug delivery systems for multiple drugs or real-time biosensors utilizing skin biomarkers.

7. Expert Opinions

MNs were conceptualized in 1971 and since then, the field of MNs have grown considerably. In terms of the transdermal market, the market growth between 2019 and 2023 is predicted to reach \$1.79 billion.^[198] With this, the World Economic Forum has included MNs as number one on the top 10 most relevant emerging technologies of 2020.^[199] Using various 3D printing methods for the fabrication of MNs has recently become more popular. Owing to several benefits of 3D printing, the fabrication of high-quality MNs with complex designs or integrated MN devices comprising of a MN and other technologies (e.g., microfluidics, electrodes, or cell microencapsulation) is now feasible. However, the capabilities of 3D printing in the fabrication of MNs could be further expanded. As previously discussed, in addition to transdermal drug delivery, MNs have been considered for a range of other applications, including therapeutic drug monitoring. To illustrate the potential of MNs, one can envisage that the outer surface of MNs fabricated by 3D printing provide an area for drugs/proteins to deposit. As a result, liquid formulations of drugs/proteins could be coated on the MNs by inkjet printing or pulsed laser deposition. In the same vein, electrospinning could be used as a coating technology for depositing solid drug formulation in the form of nano- or microfibers onto the MNs after 3D printing. In addition, by modifying the properties of polymer solution and tuning process parameters, electrospinning can be transformed to electrospraying, which, instead of generating fibers, produces minuscule particles.

The formation of personalized MN devices based on the individual physiological structures is currently possible. Commonly, MNs are designed to align on a small baseplate in a square or circular shape. With more advanced technologies and knowledge, MNs can be now fabricated on or as part of a device, such as drug eluting balloons and vascular couplers, to provide more surface area for drug coating and to diminish the inefficacy of the current treatment.^[200,201] Therefore, MN devices have potential to be applied on various organ's surfaces apart from the skin. In general, 3D printing systems are becoming more affordable, therefore, 3D printers are now more

accessible to people. Nowadays there are also 3D printers in several hospitals for crafting parts of some medical devices or even making personalized treatment such as 3D printed casts for patients. In this regard, a common 3D printing method, like FDM, can be used. On the other hand, the production of MNs is too demanding for the common method to be used, as it requires much higher resolution to achieve appropriate MN sharpness. Furthermore, the materials used in the 3D printing process must also provide satisfying mechanical strength after the production process to obtain strong MNs. Currently, most of affordable printers are FDM- and SLA-based printers (see Table 4). Although the materials used with these printers possess strong mechanical strength, they lack the ability to produce well-defined structures like MNs, especially the sharp tips that require high precision. As a result, the higher-resolution 3D printing methods that can accommodate such requirements are significantly more expensive and time consuming. In addition, the majority of these systems (e.g., TPP and CLIP) require photosensitive resins reducing the selection of available materials. This is an important limitation as these techniques can produce sharp solid MN arrays or hollow MNs. Accordingly, in order to use these devices to deliver drugs/vaccines they need to be coated into the surface, use a “poke with patch” approach or, for hollow MNs, directly injecting a formulation. This is a significant limitation considering that a large portion of MN applications described for drug/vaccine delivery use dissolving MN system. Currently, the only possible ways of producing a dissolvable 3D printed objects using water-soluble polymers, such as PVA, PVP or other pharmaceutical excipients, are extrusion-based technique^[3,202,203] or SLS.^[204] However, these types of 3D printing technologies present limitations in terms of resolution to prepare MN arrays. Additionally, to incorporate the therapeutic compound into this type of systems high temperatures are required that could potentially damage the cargo. Accordingly, there is a clear need to improve available 3D printing techniques to be able to prepare dissolving MN arrays.

In addition to the technical limitations described in the previous paragraph there are some extra hurdles that must be overcome before 3D printed MNs can transition from the laboratory to the end-user. These can be categorized into three groups: safety, acceptability, and regulatory. Although these hurdles have been previously discussed elsewhere,^[205,206] their focuses have not specifically been toward 3D printing. The safety of MNs is crucial to the acceptance by both healthcare providers and patients. To the best of our knowledge, there are currently no studies that directly investigate the safety of MNs fabricated using a 3D printer. Despite previous safety studies demonstrating that the risk of a skin infection caused by MNs is minimal,^[96,207,208] ultimately, the safety studies need to be investigated to confirm the implication of MNs fabricated by 3D printing. The US FDA has issued a guidance for industry and food and drug administration staff regarding regulatory considerations for microneedling products in November 2020. This guidance suggests that safety data should be collected in a clinical study to ensure that use of the MN device is safe. The safety data include the risks of infection, nerve and blood vessel damage, scar formation, hyper-/hypo-pigmentation, skin inflammation, allergic reactions, skin irritation, and other adverse events related to the use of the MN device.^[209] Although

the guidance recommends the manufacturers to consider the risk of skin infection from the use of MN device, it is unclear whether the final product will need to be sterilized, prepared under aseptic conditions, or simply host a low bioburden. If the sterilization or use of aseptic techniques in MN device production is a legally enforced requirement for marketing, the costs and complexity of production will considerably increase. Selecting an appropriate sterilization method will also be crucial, since the most common approaches (e.g., moist heat, gamma radiation, ethylene oxide) can cause undesirable transformation of the MNs themselves and/or any contained active ingredient (e.g., small drug molecules and biomolecules). In this regard, any contained microorganisms and pyrogens may need to be identified and quantified, and the MN device may be acceptable for use as a low bioburden product.^[210] It is important to note that the sterilization of certain types of 3D printed objects, such as PLA-based objects, can be challenging.^[211,212] However, it has been demonstrated that certain types of 3D printing techniques can be used to prepare sterile components using non-sterile materials without further sterilization steps.^[213] However, more research is needed in order to evaluate if this can be applied to the production of sterile parts under FDA regulations.

In addition, healthcare providers and patients must be willing to prescribe, use and accept MNs as an alternative pharmaceutical device. In particular, for patient acceptance, MNs must be as convenient, if not more so, than a patient's current treatment regimen. For instance, efforts have been made to assess that patients can easily self-apply MNs, with through counseling or through the use of a pressure-indicating sensor film.^[36,43,214]

Many of the studies referenced in this review demonstrate the ability of 3D printing to be used for the fabrication of MNs. Whilst it is shown that 3D printing technology offers rapid MN fabrication with high resolution and flexibility, there are specific regulatory challenges associated with 3D printed MNs. One main challenge in this regard is the commercial scale-up of 3D printed MNs. To date 3D printing is still far from perfection due to the high cost of 3D printing systems and the time that 3D printing takes to produce products in bulk. As a result, the expensive cost of using advanced printing method, like TPP, to craft high quality MNs has to be contemplated in mass-scale commercialization. 3D printed MNs can be highly useful for other applications, such as modifying the device to best suit the patient's need. This type of application can be feasible if they are applied to serious conditions such as cardiovascular disease.^[215] However, it is important to note that some materials required for 3D printing are not suitable for human use due to toxicity. Furthermore, the fabrication methods which are based on the exposure to light or using heat could accelerate the degradation of drugs and biomolecules. In this regard, blending drugs or biomolecules with printing materials can be challenging. For FDM-based printers, organic solvents are generally required to dissolve most of polymeric filaments or pellets to homogeneously mix with drugs or biomolecules. Moreover, there will be an additional step to reproduce filaments with specifically defined diameter from an active molecule-polymer blend using hot-melt extrusion. This heating step is prone to result in the degradation of heat-labile drugs/

biomolecules prior to printing. Another two crucial points to be considered are the dissolubility of MNs and the period, which MNs are in contact with the skin. Since most of printing materials are hydrophobic, they are less likely to be dissolved by the fluid in the skin. As a result, prolonged application time may be required to allow MNs to dissolve in order to release active drugs or biomolecules. Therefore, more appealing approaches such as using water-soluble printing materials, or coating active ingredients on the surface of MNs are more commonly used. Consequently, the selection of 3D printing methods and materials during the development of MNs should be thoroughly considered if mass production is desirable in the future. It is more likely that using 3D printing to produce a master MN, which will be subsequently used to produce molds, will be more realistic for commercialization. These molds can then be repeatedly used to produce many MNs in a short time-scale, with favorable FDA-approved polymers employed rather than toxic resins. Moreover, the molds can also function as a simple device for coating solutions (e.g., drug solution, protein solution) on the surface of MNs. By simply filling the holes of each mold with coating solution and reinserting the MNs into the molds, the coating material will be adsorbed/absorbed on the MNs depending on the types of material constituting the MNs. An alternative approach for depositing drug or protein on the surface of MNs involves an inkjet printer to precisely dispense a defined amount of drug or protein solution on the surface of MNs in a reproducible manner. With this method, dose of drug/protein can be adjusted to meet the need of the individual for their course of treatment. While the MNs bypass the SC to enhance the success of drug delivery, the compositions of coating material will determine the release rate and order of active ingredients to the skin. One limitation is possibly the amount of drug/protein that can be loaded on the surface of MNs. The thickness of the coating material should not be too thick to change the capability of skin insertion of MNs. Therefore, highly potent drugs and proteins are generally more suitable in this regard when compared to drugs/proteins with lower potency. In this case, vaccines are the most promising substances as their effective doses are relatively small (e.g., Spikevax: 50–100 µg mRNA,^[216] Comirnaty: 30 µg tozinameran,^[217] influenza vaccines: 7.5–15 µg,^[218] etc.). Other examples of potent drugs and proteins and their effective doses that have been delivered by coated MNs are pilocarpine (5.5 µg),^[219] doxorubicin (0.6 µg),^[220] desmopressin (82 µg),^[61] OVA (1 µg),^[221] and 5-aminolevulinic acid (350 µg).^[222] Therefore, the inkjet printer-mold combination is considered to be the future of MN mass manufacture.

Acknowledgements

The authors thank Wellcome Trust Grant on the 3D bioscaffold (UNS40040) for funding and thank Servier Medical Art (smart.servier.com) for figures.

Conflict of Interest

The authors declare no conflict of interest.

Keywords

3D printing, additive manufacturing, drug delivery, medical device, microneedle

Received: October 20, 2021

Revised: March 13, 2022

Published online:

- [1] T. D. Ngo, A. Kashani, G. Imbalzano, K. T. Q. Nguyen, D. Hui, *Composites, Part B* **2018**, *143*, 172.
- [2] P. Honigmann, N. Sharma, B. Okolo, U. Popp, B. Msallem, F. M. Thieringer, *Biomed Res. Int.* **2018**, *2018*, 4520636.
- [3] A. Goyanes, A. B. M. Buanz, A. W. Basit, S. Gaisford, *Int. J. Pharm.* **2014**, *476*, 88.
- [4] N. G. Solanki, M. Tahsin, A. V. Shah, A. T. M. Serajuddin, *J. Pharm. Sci.* **2018**, *107*, 390.
- [5] S. A. Khaled, J. C. Burley, M. R. Alexander, J. Yang, C. J. Roberts, *J. Controlled Release* **2015**, *217*, 308.
- [6] S. V. Murphy, A. Atala, *Nat. Biotechnol.* **2014**, *32*, 773.
- [7] N. K. Martin, J. Domínguez-Robles, S. A. Stewart, V. A. Cornelius, Q. K. Anjani, E. Utomo, I. García-Romero, R. F. Donnelly, A. Margariti, D. A. Lamprou, E. Larrañeta, *Int. J. Pharm.* **2021**, *595*, 120243.
- [8] J. Domínguez-Robles, C. Mancinelli, E. Mancuso, I. García-Romero, B. F. Gilmore, L. Casettari, E. Larrañeta, D. A. Lamprou, *Pharmaceutics* **2020**, *12*, 63.
- [9] Z. L. Farmer, E. Utomo, J. Domínguez-Robles, C. Mancinelli, E. Mathew, E. Larrañeta, D. A. Lamprou, *Int. J. Pharm.* **2021**, *593*, 120145.
- [10] J. Domínguez-Robles, T. Shen, V. A. Cornelius, F. Corduas, E. Mancuso, R. F. Donnelly, A. Margariti, D. A. Lamprou, E. Larrañeta, *Mater. Sci. Eng. C* **2021**, *129*, 112375.
- [11] J. Wang, A. Goyanes, S. Gaisford, A. W. Basit, *Int. J. Pharm.* **2016**, *503*, 207.
- [12] X. Xu, P. Robles-Martinez, C. M. Madla, F. Joubert, A. Goyanes, A. W. Basit, S. Gaisford, *Addit. Manuf.* **2020**, *33*, 101071.
- [13] R. Thakkar, Y. Zhang, J. Zhang, M. Maniruzzaman, *Eur. J. Pharm. Biopharm.* **2021**, *163*, 141.
- [14] L. K. Prasad, H. Smyth, *Drug Dev. Ind. Pharm.* **2016**, *42*, 1019.
- [15] S. E. Moulton, G. G. Wallace, *J. Controlled Release* **2014**, *193*, 27.
- [16] W. Jamróz, J. Szafraniec, M. Kurek, R. Jachowicz, *Pharm. Res.* **2018**, *35*, 176.
- [17] S. A. Stewart, J. Domínguez-Robles, V. J. McIlorum, Z. Gonzalez, E. Utomo, E. Mancuso, D. A. Lamprou, R. F. Donnelly, E. Larrañeta, *Mol. Pharmaceutics* **2020**, *17*, 3487.
- [18] S. Stewart, J. Domínguez-Robles, V. McIlorum, E. Mancuso, D. Lamprou, R. Donnelly, E. Larrañeta, *Pharmaceutics* **2020**, *12*, 105.
- [19] E. Mathew, J. Domínguez-Robles, S. A. Stewart, E. Mancuso, K. O'Donnell, E. Larrañeta, D. A. Lamprou, *ACS Biomater. Sci. Eng.* **2019**, *5*, 6300.
- [20] G. R. J. Swennen, L. Pottel, P. E. Haers, *Int. J. Oral Maxillofac. Surg.* **2020**, *49*, 673.
- [21] E. Larrañeta, J. Dominguez-Robles, D. A. Lamprou, *3D Print. Addit. Manuf.* **2020**, *7*, 100.
- [22] S. C. Ligon, R. Liska, J. Stampfl, M. Gurr, R. Mühlaupt, *Chem. Rev.* **2017**, *117*, 10212.
- [23] A. Goyanes, U. Det-Amornrat, J. Wang, A. W. Basit, S. Gaisford, *J. Controlled Release* **2016**, *234*, 41.
- [24] J. W. Stansbury, M. J. Idacavage, *Dent. Mater.* **2016**, *32*, 54.
- [25] M. F. Attia, B. R. Brummel, T. R. Lex, B. A. Van Horn, D. C. Whitehead, F. Alexis, *Adv. Healthcare Mater.* **2018**, *7*, 1800798.
- [26] D. Mitsouras, T. C. Lee, P. Liacouras, C. N. Ionita, T. Pietilla, S. E. Maier, R. V. Mulkern, *Magn. Reson. Med.* **2017**, *77*, 613.
- [27] T. M. Bücking, E. R. Hill, J. L. Robertson, E. Maneas, A. A. Plumb, D. I. Nikitichev, *PLoS One* **2017**, *12*, e0178540.
- [28] Q. Yan, H. Dong, J. Su, J. Han, B. Song, Q. Wei, Y. Shi, *Engineering* **2018**, *4*, 729.
- [29] T.-M. Tuan-Mahmood, M. T. C. McCrudden, B. M. Torrisi, E. McAlister, M. J. Garland, T. R. R. Singh, R. F. Donnelly, *Eur. J. Pharm. Sci.* **2013**, *50*, 623.
- [30] E. Larrañeta, R. E. M. Lutton, A. D. Woolfson, R. F. Donnelly, *Mater. Sci. Eng., R* **2016**, *104*, 1.
- [31] Y.-C. Kim, J.-H. Park, M. R. Prausnitz, *Adv. Drug Delivery Rev.* **2012**, *64*, 1547.
- [32] T. Waghule, G. Singhvi, S. K. Dubey, M. M. Pandey, G. Gupta, M. Singh, K. Dua, *Biomed. Pharmacother.* **2019**, *109*, 1249.
- [33] R. F. Donnelly, E. Larrañeta, *Drug Discovery Today* **2018**, *23*, 1026.
- [34] H. S. Gill, D. D. Denson, B. A. Burriss, M. R. Prausnitz, *Clin. J. Pain* **2008**, *24*, 585.
- [35] J. C. Birchall, R. Clemo, A. Anstey, D. N. John, *Pharm. Res.* **2011**, *28*, 95.
- [36] R. F. Donnelly, K. Moffatt, A. Z. Alkilani, E. M. Vicente-Pérez, J. Barry, M. T. C. McCrudden, A. D. Woolfson, *Pharm. Res.* **2014**, *31*, 1989.
- [37] T. M. Rawson, S. A. N. Gowers, D. M. E. Freeman, R. C. Wilson, S. Sharma, M. Gilchrist, A. MacGowan, A. Lovering, M. Bayliss, M. Kyriakides, P. Georgiou, A. E. G. Cass, D. O'Hare, A. H. Holmes, *Lancet Digital Heal.* **2019**, *1*, e335.
- [38] D. H. Keum, H. S. Jung, T. Wang, M. H. Shin, Y.-E. Kim, K. H. Kim, G.-O. Ahn, S. K. Hahn, *Adv. Healthcare Mater.* **2015**, *4*, 1153.
- [39] P. R. Miller, X. Xiao, I. Brener, D. B. Burckel, R. Narayan, R. Polsky, *Adv. Healthcare Mater.* **2014**, *3*, 876.
- [40] R. F. Donnelly, T. R. R. Singh, M. M. Tunney, D. I. J. Morrow, P. A. McCarron, C. O'Mahony, A. D. Woolfson, *Pharm. Res.* **2009**, *26*, 2513.
- [41] T. Orenius, LicPsych, H. Säilä, K. Mikola, L. Ristolainen, *SAGE Open Nurs.* **2018**, *4*, 237796081875944.
- [42] J. McLenon, M. A. M. Rogers, *J. Adv. Nurs.* **2019**, *75*, 30.
- [43] E. M. Vicente-Pérez, H. L. Quinn, E. McAlister, S. O'Neill, L.-A. Hanna, J. G. Barry, R. F. Donnelly, *Pharm. Res.* **2016**, *33*, 3072.
- [44] A. R. Johnson, A. T. Procopio, *3D Print. Med.* **2019**, *5*, 2.
- [45] C. P. P. Pere, S. N. Economidou, G. Lall, C. Ziraud, J. S. Boateng, B. D. Alexander, D. A. Lamprou, D. Douroumis, *Int. J. Pharm.* **2018**, *544*, 425.
- [46] C. Yeung, S. Chen, B. King, H. Lin, K. King, F. Akhtar, G. Diaz, B. Wang, J. Zhu, W. Sun, A. Khademhosseini, S. Emaminejad, *Biomicrofluidics* **2019**, *13*, 064125.
- [47] A. R. Johnson, C. L. Caudill, J. R. Tumbleston, C. J. Bloomquist, K. A. Moga, A. Ermoshkin, D. Shirvanyants, S. J. Mecham, J. C. Luft, J. M. De Simone, *PLoS One* **2016**, *11*, e016251.
- [48] K. J. Krieger, N. Bertollo, M. Dangol, J. T. Sheridan, M. M. Lowery, E. D. O'Ceirbhail, *Microsyst. Nanoeng.* **2019**, *5*, 42.
- [49] D. Han, R. S. Morde, S. Mariani, A. A. La Mattina, E. Vignali, C. Yang, G. Barillaro, H. Lee, *Adv. Funct. Mater.* **2020**, *30*, 1909197.
- [50] R. D. Boehm, P. R. Miller, R. Singh, A. Shah, S. Stafslie, J. Daniels, R. J. Narayan, *Biofabrication* **2012**, *4*, 011002.
- [51] Jung-Hwan Park, Yong-Kyu Yoon, Seong-O Choi, M. R. Prausnitz, M. G. Allen, *IEEE Trans. Biomed. Eng.* **2007**, *54*, 903.
- [52] J. W. Lee, M.-R. Han, J.-H. Park, *J. Drug Targeting* **2013**, *21*, 211.
- [53] J.-H. Park, M. G. Allen, M. R. Prausnitz, *J. Controlled Release* **2005**, *104*, 51.
- [54] S. Park, M. Kim, S.-K. Baek, J.-H. Park, S.-O. Choi, *Polymers* **2019**, *11*, 369.
- [55] W. Martanto, S. P. Davis, N. R. Holiday, J. Wang, H. S. Gill, M. R. Prausnitz, *Pharm. Res.* **2004**, *21*, 947.

- [56] D. V. McAllister, P. M. Wang, S. P. Davis, J.-H. Park, P. J. Canatella, M. G. Allen, M. R. Prausnitz, *Proc. Natl. Acad. Sci. USA* **2003**, *100*, 13755.
- [57] Q. Y. Li, J. N. Zhang, B. Z. Chen, Q. L. Wang, X. D. Guo, *RSC Adv.* **2017**, *7*, 15408.
- [58] J. Gupta, H. S. Gill, S. N. Andrews, M. R. Prausnitz, *J. Controlled Release* **2011**, *154*, 148.
- [59] X. He, J. Sun, J. Zhuang, H. Xu, Y. Liu, D. Wu, *Dose-Response* **2019**, *17*, 155932581987858.
- [60] C. Tas, S. Mansoor, H. Kalluri, V. G. Zarnitsyn, S. O. Choi, A. K. Banga, M. R. Prausnitz, *Int. J. Pharm.* **2012**, *423*, 257.
- [61] M. Cormier, B. Johnson, M. Ameri, K. Nyam, L. Libiran, D. D. Zhang, P. Daddona, *J. Controlled Release* **2004**, *97*, 503.
- [62] P. E. Daddona, J. A. Matriano, J. Mandema, Y.-F. Maa, *Pharm. Res.* **2011**, *28*, 159.
- [63] H. S. Lee, H. R. Ryu, J. Y. Roh, J.-H. Park, *Pharm. Res.* **2017**, *34*, 101.
- [64] S.-H. Baek, J.-H. Shin, Y.-C. Kim, *Biomed. Microdevices* **2017**, *19*, 2.
- [65] H. L. Quinn, R. F. Donnelly, in *Microneedles for Drug and Vaccine Delivery and Patient Monitoring* (Eds: R. F. Donnelly, T. R. R. Singh, E. Larrañeta, M. T. C. McCrudden), John Wiley & Sons, Inc, Chichester, West Sussex **2018**, pp. 71–91.
- [66] Y.-C. Kim, F.-S. Quan, J.-M. Song, A. Vunnavu, D.-G. Yoo, K.-M. Park, R. W. Compans, S.-M. Kang, M. R. Prausnitz, *Procedia Vaccinol.* **2010**, *2*, 17.
- [67] J. Chen, Y. Qiu, S. Zhang, G. Yang, Y. Gao, *Drug Dev. Ind. Pharm.* **2015**, *41*, 415.
- [68] M. J. Garland, E. Caffarel-Salvador, K. Migalska, A. D. Woolfson, R. F. Donnelly, *J. Controlled Release* **2012**, *159*, 52.
- [69] B. Pamornpathomkul, T. Ngawhirunpat, I. A. Tekko, L. Vora, H. O. McCarthy, R. F. Donnelly, *Eur. J. Pharm. Sci.* **2018**, *121*, 200.
- [70] M. T. C. McCrudden, A. Z. Alkilani, C. M. McCrudden, E. McAlister, H. O. McCarthy, A. D. Woolfson, R. F. Donnelly, *J. Controlled Release* **2014**, *180*, 71.
- [71] A. R. J. Hutton, P. L. Quinn, P. J. McCague, C. Jarrahan, A. Rein-Weston, H. S. Coffey, E. Gerth-Guyette, D. Zehring, E. Larrañeta, R. F. Donnelly, *Int. J. Pharm.* **2018**, *541*, 56.
- [72] P. González-Vázquez, E. Larrañeta, M. T. C. McCrudden, C. Jarrahan, A. Rein-Weston, M. Quintanar-Solares, D. Zehring, H. McCarthy, A. J. Courtenay, R. F. Donnelly, *J. Controlled Release* **2017**, *265*, 30.
- [73] E. Larrañeta, S. Stewart, S. J. Fallows, L. L. Birkhäuser, M. T. C. McCrudden, A. D. Woolfson, R. F. Donnelly, *Int. J. Pharm.* **2016**, *497*, 62.
- [74] K. Migalska, D. I. J. Morrow, M. J. Garland, R. Thakur, A. D. Woolfson, R. F. Donnelly, *Pharm. Res.* **2011**, *28*, 1919.
- [75] Y. Ito, A. Murakami, T. Maeda, N. Sugioka, K. Takada, *Int. J. Pharm.* **2008**, *349*, 124.
- [76] Y. A. Goma, M. J. Garland, F. McInnes, L. K. El-Khordagui, C. Wilson, R. F. Donnelly, *Eur. J. Pharm. Biopharm.* **2012**, *82*, 299.
- [77] Y. Ito, K. Shirogama, J. Yoshimitsu, Y. Ohashi, N. Sugioka, K. Takada, *J. Controlled Release* **2007**, *121*, 176.
- [78] J. W. Lee, S.-O. Choi, E. I. Felner, M. R. Prausnitz, *Small* **2011**, *7*, 531.
- [79] K. Ita, *Biomed. Pharmacother.* **2017**, *93*, 1116.
- [80] P. M. Wang, M. Cornwell, J. Hill, M. R. Prausnitz, *J. Invest. Dermatol.* **2006**, *126*, 1080.
- [81] J. D. Brazzle, I. Papautsky, A. B. Frazier, *Biomed. Microdevices* **2000**, *2*, 197.
- [82] P. Griss, G. Stemme, *J. Microelectromech. Syst.* **2003**, *12*, 296.
- [83] R. F. Donnelly, T. R. R. Singh, M. J. Garland, K. Migalska, R. Majithiya, C. M. McCrudden, P. L. Kole, T. M. T. Mahmood, H. O. McCarthy, A. D. Woolfson, *Adv. Funct. Mater.* **2012**, *22*, 4879.
- [84] R. F. Donnelly, M. T. C. McCrudden, A. Zaid Alkilani, E. Larrañeta, E. McAlister, A. J. Courtenay, M.-C. Kearney, T. R. R. Singh, H. O. McCarthy, V. L. Kett, E. Caffarel-Salvador, S. Al-Zahrani, A. D. Woolfson, *PLoS One* **2014**, *9*, e111547.
- [85] E. McAlister, B. Dutton, L. K. Vora, L. Zhao, A. Ripolin, D. S. Z. B. P. H. Zahari, H. L. Quinn, I. A. Tekko, A. J. Courtenay, S. A. Kelly, A. M. Rodgers, L. Steiner, G. Levin, E. Levy-Nissenbaum, N. Shterman, H. O. McCarthy, R. F. Donnelly, *Adv. Healthcare Mater.* **2021**, *10*, 2001256.
- [86] E. M. Migdadi, A. J. Courtenay, I. A. Tekko, M. T. C. McCrudden, M.-C. Kearney, E. McAlister, H. O. McCarthy, R. F. Donnelly, *J. Controlled Release* **2018**, *285*, 142.
- [87] A. J. Courtenay, M. T. C. McCrudden, K. J. McAvoy, H. O. McCarthy, R. F. Donnelly, *Mol. Pharmaceutics* **2018**, *15*, 3545.
- [88] A. J. Courtenay, E. McAlister, M. T. C. McCrudden, L. Vora, L. Steiner, G. Levin, E. Levy-Nissenbaum, N. Shterman, M. Shterman, H. O. McCarthy, R. F. Donnelly, *J. Controlled Release* **2020**, *322*, 177.
- [89] M.-C. Kearney, E. Caffarel-Salvador, S. J. Fallows, H. O. McCarthy, R. F. Donnelly, *Eur. J. Pharm. Biopharm.* **2016**, *103*, 43.
- [90] S. Y. Yang, E. D. O’Cearbhaill, G. C. Sisk, K. M. Park, W. K. Cho, M. Villiger, B. E. Bouma, B. Pomahac, J. M. Karp, *Nat. Commun.* **2013**, *4*, 1702.
- [91] J. G. Turner, L. R. White, P. Estrela, H. S. Leese, *Macromol. Biosci.* **2021**, *21*, 2000307.
- [92] R. He, Y. Niu, Z. Li, A. Li, H. Yang, F. Xu, F. Li, *Adv. Healthcare Mater.* **2020**, *9*, 1901201.
- [93] A. Than, C. Liu, H. Chang, P. K. Duong, C. M. G. Cheung, C. Xu, X. Wang, P. Chen, *Nat. Commun.* **2018**, *9*, 4433.
- [94] Z. Yin, D. Kuang, S. Wang, Z. Zheng, V. K. Yadavalli, S. Lu, *Int. J. Biol. Macromol.* **2018**, *106*, 48.
- [95] H. Chang, M. Zheng, X. Yu, A. Than, R. Z. Seeni, R. Kang, J. Tian, D. P. Khanh, L. Liu, P. Chen, C. Xu, *Adv. Mater.* **2017**, *29*, 1702243.
- [96] R. Al-Kasasbeh, A. J. Brady, A. J. Courtenay, E. Larrañeta, M. T. C. McCrudden, D. O’Kane, S. Liggett, R. F. Donnelly, *Drug Delivery Transl. Res.* **2020**, *10*, 690.
- [97] E. Caffarel-Salvador, A. J. Brady, E. Eltayib, T. Meng, A. Alonso-Vicente, P. Gonzalez-Vazquez, B. M. Torrisi, E. M. Vicente-Perez, K. Mooney, D. S. Jones, S. E. J. Bell, C. P. McCoy, H. O. McCarthy, J. C. McElroy, R. F. Donnelly, *PLoS One* **2015**, *10*, e0145644.
- [98] B. Al-Qallaf, D. B. Das, *J. Drug Targeting* **2009**, *17*, 108.
- [99] S. D. Gittard, B. Chen, H. Xu, A. Ovsianikov, B. N. Chichkov, N. A. Monteiro-Riviere, R. J. Narayan, *J. Adhes. Sci. Technol.* **2013**, *27*, 227.
- [100] S. P. Davis, B. J. Landis, Z. H. Adams, M. G. Allen, M. R. Prausnitz, *J. Biomech.* **2004**, *37*, 1155.
- [101] A. Davidson, B. Al-Qallaf, D. B. Das, *Chem. Eng. Res. Des.* **2008**, *86*, 1196.
- [102] R. F. Donnelly, M. J. Garland, D. I. J. Morrow, K. Migalska, T. R. R. Singh, R. Majithiya, A. D. Woolfson, *J. Controlled Release* **2010**, *147*, 333.
- [103] E. Z. Loizidou, N. T. Inoue, J. Ashton-Barnett, D. A. Barrow, C. J. Allender, *Eur. J. Pharm. Biopharm.* **2016**, *107*, 1.
- [104] M. A. Luzziaga, D. R. Berry, J. C. Reagan, R. A. Smaldone, J. J. Gassensmith, *Lab Chip* **2018**, *18*, 1223.
- [105] M. Ochoa, J. Zhou, R. Rahimi, V. Badwaik, D. Thompson, B. Ziaie, in *2015 Transducers –2015 18th Int. Conf. Solid-State Sensors, Actuators Microsystems*, IEEE, Piscataway, NJ **2015**, pp. 1251–1254..
- [106] S. N. Economidou, C. P. P. Pere, A. Reid, M. J. Uddin, J. F. C. Windmill, D. A. Lamprou, D. Douroumis, *Mater. Sci. Eng. C* **2019**, *102*, 743.
- [107] M. J. Uddin, N. Scutaris, S. N. Economidou, C. Giraud, B. Z. Chowdhry, R. F. Donnelly, D. Douroumis, *Mater. Sci. Eng. C* **2020**, *107*, 110248.
- [108] M. A. Lopez-Ramirez, F. Soto, C. Wang, R. Rueda, S. Shukla, C. Silva-Lopez, D. Kupor, D. A. McBride, J. K. Pokorski,

- A. Nourhani, N. F. Steinmetz, N. J. Shah, J. Wang, *Adv. Mater.* **2020**, *32*, 1905740.
- [109] A. Doraiswamy, C. Jin, R. Narayan, P. Mageswaran, P. Mente, R. Modi, R. Auyeung, D. Chrisey, A. Ovsianikov, B. Chichkov, *Acta Biomater.* **2006**, *2*, 267.
- [110] A. Ovsianikov, B. Chichkov, P. Mente, N. A. Monteiro-Riviere, A. Doraiswamy, R. J. Narayan, *Int. J. Appl. Ceram. Technol.* **2007**, *4*, 22.
- [111] S. D. Gittard, A. Ovsianikov, N. A. Monteiro-Riviere, J. Lusk, P. Morel, P. Minghetti, C. Lenardi, B. N. Chichkov, R. J. Narayan, *J. Diabetes Sci. Technol.* **2009**, *3*, 304.
- [112] S. D. Gittard, R. J. Narayan, C. Jin, A. Ovsianikov, B. N. Chichkov, N. A. Monteiro-Riviere, S. Stafslin, B. Chisholm, *Biofabrication* **2009**, *1*, 041001.
- [113] S. D. Gittard, A. Ovsianikov, H. Akar, B. Chichkov, N. A. Monteiro-Riviere, S. Stafslin, B. Chisholm, C.-C. Shin, C.-M. Shih, S.-J. Lin, Y.-Y. Su, R. J. Narayan, *Adv. Eng. Mater.* **2010**, *12*, B77.
- [114] M. Kavaldzhiev, J. E. Perez, Y. Ivanov, A. Bertoncini, C. Liberale, J. Kosel, *Biomed. Phys. Eng. Express* **2017**, *3*, 025005.
- [115] K. Moussi, A. Bukhamsin, T. Hidalgo, J. Kosel, *Adv. Eng. Mater.* **2020**, *22*, 2070005.
- [116] S. H. Lim, J. Y. Ng, L. Kang, *Biofabrication* **2017**, *9*, 015010.
- [117] W. Yao, D. Li, Y. Zhao, Z. Zhan, G. Jin, H. Liang, R. Yang, *Micromachines* **2019**, *11*, 17.
- [118] J. Choi, I. Park, Y. Ha, M. Jung, S. Lee, S. Lee, in *2006 SICE-ICASE Int. Joint Conf.*, IEEE, Piscataway, NJ **2006**, pp. 3678–3681.
- [119] S. D. Gittard, P. R. Miller, C. Jin, T. N. Martin, R. D. Boehm, B. J. Chisholm, S. J. Stafslin, J. W. Daniels, N. Cilz, N. A. Monteiro-Riviere, A. Nasir, R. J. Narayan, *JOM* **2011**, *63*, 59.
- [120] H. Yun, H. Kim, *J. Mech. Sci. Technol.* **2013**, *27*, 2973.
- [121] Y. Lu, S. N. Mantha, D. C. Crowder, S. Chinchilla, K. N. Shah, Y. H. Yun, R. B. Wicker, J.-W. Choi, *Biofabrication* **2015**, *7*, 045001.
- [122] R. D. Boehm, P. R. Miller, S. L. Hayes, N. A. Monteiro-Riviere, R. J. Narayan, *AIP Adv.* **2011**, *1*, 022139.
- [123] M. Gieseke, V. Senz, M. Vehse, S. Fiedler, R. Irsig, M. Hustedt, K. Sternberg, C. Nölke, S. Kaierle, V. Wesling, J. Tiggesbäumker, K.-H. Meiwes-Broer, H. Seitz, K.-P. Schmitz, H. Haferkamp, *Biomed. Eng./Biomed. Tech.* **2012**, *57*, 398.
- [124] R. M. Cardoso, C. Kalinke, R. G. Rocha, P. L. dos Santos, D. P. Rocha, P. R. Oliveira, B. C. Janegitz, J. A. Bonacin, E. M. Richter, R. A. A. Munoz, *Anal. Chim. Acta* **2020**, *1118*, 73.
- [125] A. Goyanes, A. B. M. Buanz, G. B. Hatton, S. Gaisford, A. W. Basit, *Eur. J. Pharm. Biopharm.* **2015**, *89*, 157.
- [126] K. Tappa, U. Jammalamadaka, *J. Funct. Biomater.* **2018**, *9*, 17.
- [127] J. S. Chohan, R. Singh, K. S. Boparai, R. Penna, F. Fraternali, *Composites, Part B* **2017**, *117*, 138.
- [128] V. Mazzanti, L. Malagutti, F. Mollica, *Polymers* **2019**, *11*, 1094.
- [129] E. G. Gordeev, A. S. Galushko, V. P. Ananikov, *PLoS One* **2018**, *13*, e0198370.
- [130] K. Takagishi, S. Umezu, *Sci. Rep.* **2017**, *7*, 39852.
- [131] A. Vitale, J. Cabral, *Materials* **2016**, *9*, 760.
- [132] K. Szykiedans, W. Credo, *Procedia Eng.* **2016**, *136*, 257.
- [133] S. Ahn, M. Montero, D. Odell, S. Roundy, P. K. Wright, *Rapid Prototyping J.* **2002**, *8*, 248.
- [134] S. Garzon-Hernandez, D. Garcia-Gonzalez, A. Jérusalem, A. Arias, *Mater. Des.* **2020**, *188*, 108414.
- [135] M. A. Alhnan, T. C. Okwuosa, M. Sadia, K.-W. Wan, W. Ahmed, B. Ararat, *Pharm. Res.* **2016**, *33*, 1817.
- [136] S. M. Saptarshi, D. C. Zhou, in *3D Printing in Orthopaedic Surgery*, (Eds: M. Dipaola, F. M. Wodajo), Elsevier, Amsterdam **2019**, pp. 17–30.
- [137] G. Taormina, C. Sciancalepore, M. Messori, F. Bondioli, *J. Appl. Biomater. Funct. Mater.* **2018**, *16*, 151.
- [138] E. A. Garcia, C. Ayranci, A. J. Qureshi, *J. Manuf. Mater. Process.* **2020**, *4*, 12.
- [139] Y. Yang, L. Li, J. Zhao, *Mater. Des.* **2019**, *162*, 418.
- [140] K. B. Vinayakumar, P. G. Kulkarni, M. M. Nayak, N. S. Dinesh, G. M. Hegde, S. G. Ramachandra, K. Rajanna, *J. Microeng. Microeng.* **2016**, *26*, 065013.
- [141] S. J. Moon, S. S. Lee, H. S. Lee, T. H. Kwon, *Microsyst. Technol.* **2005**, *11*, 311.
- [142] S. P. Sullivan, N. Murthy, M. R. Prausnitz, *Adv. Mater.* **2008**, *20*, 933.
- [143] K. Kim, D. S. Park, H. M. Lu, W. Che, K. Kim, J.-B. Lee, C. H. Ahn, *J. Microeng. Microeng.* **2004**, *14*, 597.
- [144] H. R. Nejad, A. Sadeqi, G. Kiaee, S. Sonkusale, *Microsyst. Nanoeng.* **2018**, *4*, 17073.
- [145] H. Juster, B. Aar, H. Brouwer, *Polym. Eng. Sci.* **2019**, *59*, 877.
- [146] Z. Weng, Y. Zhou, W. Lin, T. Senthil, L. Wu, *Composites, Part A* **2016**, *88*, 234.
- [147] J. Borrello, P. Nasser, J. C. Iatridis, K. D. Costa, *Addit. Manuf.* **2018**, *23*, 374.
- [148] H. Quan, T. Zhang, H. Xu, S. Luo, J. Nie, X. Zhu, *Bioact. Mater.* **2020**, *5*, 110.
- [149] X. Wang, M. Jiang, Z. Zhou, J. Gou, D. Hui, *Composites, Part B* **2017**, *110*, 442.
- [150] C. Hart, C. M. Didier, F. Sommerhage, S. Rajaraman, *Biosensors* **2020**, *10*, 152.
- [151] N. P. Macdonald, F. Zhu, C. J. Hall, J. Reboud, P. S. Crosier, E. E. Patton, D. Wlodkowic, J. M. Cooper, *Lab Chip* **2016**, *16*, 291.
- [152] H. B. Rogers, L. T. Zhou, A. Kusuhara, E. Zaniker, S. Shafaie, B. C. Owen, F. E. Duncan, T. K. Woodruff, *Chemosphere* **2021**, *270*, 129003.
- [153] S. Kreß, R. Schaller-Ammann, J. Feiel, J. Priedl, C. Kasper, D. Egger, *Materials* **2020**, *13*, 3011.
- [154] C. Kurzmann, K. Janjić, H. Shokoohi-Tabrizi, M. Edelmayer, M. Pensch, A. Moritz, H. Agis, *Biomed. Res. Int.* **2017**, *2017*, 4057612.
- [155] M. Carve, D. Wlodkowic, *Micromachines* **2018**, *9*, 91.
- [156] S. D. Gittard, A. Ovsianikov, B. N. Chichkov, A. Doraiswamy, R. J. Narayan, *Expert Opin. Drug Delivery* **2010**, *7*, 513.
- [157] X. Zhou, Y. Hou, J. Lin, *AIP Adv.* **2015**, *5*, 030701.
- [158] A. S. Cordeiro, I. A. Tekko, M. H. Jomaa, L. Vora, E. McAlister, F. Volpe-Zanutto, M. Nethery, P. T. Baine, N. Mitchell, D. W. McNeill, R. F. Donnelly, *Pharm. Res.* **2020**, *37*, 174.
- [159] S. H. Bariya, M. C. Gohel, T. A. Mehta, O. P. Sharma, *J. Pharm. Pharmacol.* **2011**, *64*, 11.
- [160] C. LaFratta, T. Baldacchini, *Micromachines* **2017**, *8*, 101.
- [161] J. R. Tumbleston, D. Shirvanyants, N. Ermoshkin, R. Januszewicz, A. R. Johnson, D. Kelly, K. Chen, R. Pinschmidt, J. P. Rolland, A. Ermoshkin, E. T. Samulski, J. M. DeSimone, *Science* **2015**, *347*, 1349.
- [162] S. R. Dabbagh, M. R. Sarabi, R. Rahbarghazi, E. Sokullu, A. K. Yetisen, S. Tasoglu, *iScience* **2021**, *24*, 102012.
- [163] Z. Chen, X. Wu, D. Tomus, C. H. J. Davies, *Addit. Manuf.* **2018**, *21*, 91.
- [164] P. K. Gokuldoss, S. Kolla, J. Eckert, *Materials* **2017**, *10*, 672.
- [165] Y. Kaynak, O. Kitay, *Addit. Manuf.* **2019**, *26*, 84.
- [166] L. Löber, C. Flache, R. Petters, U. Kühn, J. Eckert, *Rapid Prototyping J.* **2013**, *19*, 173.
- [167] A. M. Römgens, D. L. Bader, J. A. Bouwstra, F. P. T. Baaijens, C. W. J. Oomens, *J. Mech. Behav. Biomed. Mater.* **2014**, *40*, 397.
- [168] P. Khanna, K. Luongo, J. A. Strom, S. Bhansali, *J. Microeng. Microeng.* **2010**, *20*, 045011.
- [169] E. George, P. Liacouras, F. J. Rybicki, D. Mitsouras, *RadioGraphics* **2017**, *37*, 1424.
- [170] Z.-X. Low, Y. T. Chua, B. M. Ray, D. Mattia, I. S. Metcalfe, D. A. Patterson, *J. Membr. Sci.* **2017**, *523*, 596.

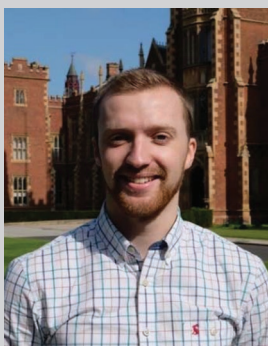
- [171] Q. Ge, Z. Li, Z. Wang, K. Kowsari, W. Zhang, X. He, J. Zhou, N. X. Fang, *Int. J. Extreme Manuf.* **2020**, 2, 022004.
- [172] C. L. Lay, C. S. L. Koh, Y. H. Lee, G. C. Phan-Quang, H. Y. F. Sim, S. X. Leong, X. Han, I. Y. Phang, X. Y. Ling, *ACS Appl. Mater. Interfaces* **2020**, 12, 10061.
- [173] V. Gupta, P. Nesterenko, B. Paull, in *3D Printing in Chemical Sciences*, (Eds: V. Gupta, P. Nesterenko, B. Paull), Royal Society of Chemistry, Cambridge **2019**, pp. 1–21.
- [174] Formlabs and Greenlight guru, “The ultimate guide to quality assurance and regulatory affairs in medical 3D printing,” <https://www.greenlight.guru/blog/medical-device-3d-printing> (accessed: March 2022).
- [175] Y. Zhou, W. M. Huang, S. F. Kang, X. L. Wu, H. B. Lu, J. Fu, H. Cui, *J. Mech. Sci. Technol.* **2015**, 29, 4281.
- [176] J. Choi, O.-C. Kwon, W. Jo, H. J. Lee, M.-W. Moon, *3D Print. Addit. Manuf.* **2015**, 2, 159.
- [177] C. Farias, R. Lyman, C. Hemingway, H. Chau, A. Mahacek, E. Bouzos, M. Mobed-Miremadi, *Bioengineering* **2018**, 5, 59.
- [178] Z. Faraji Rad, R. E. Nordon, C. J. Anthony, L. Bilston, P. D. Prewett, J.-Y. Arns, C. H. Arns, L. Zhang, G. J. Davies, *Microsyst. Nanoeng.* **2017**, 3, 17034.
- [179] A. Trautmann, G.-L. Roth, B. Nujiqi, T. Walther, R. Hellmann, *Microsyst. Nanoeng.* **2019**, 5, 6.
- [180] P. R. Miller, S. D. Gittard, T. L. Edwards, D. A. M. Lopez, X. Xiao, D. R. Wheeler, N. A. Monteiro-Riviere, S. M. Brozik, R. Polsky, R. J. Narayan, *Biomicrofluidics* **2011**, 5, 013415.
- [181] P. R. Miller, S. A. Skoog, T. L. Edwards, D. M. Lopez, D. R. Wheeler, D. C. Arango, X. Xiao, S. M. Brozik, J. Wang, R. Polsky, R. J. Narayan, *Talanta* **2012**, 88, 739.
- [182] J. X. J. Zhang, K. Hoshino, in *Molecular Sensors and Nanodevices*, (Eds: J. X. J. Zhang, K. Hoshino), Elsevier, Amsterdam **2014**, pp. 103–168.
- [183] A. D. van der Meer, A. A. Poot, M. H. G. Duits, J. Feijen, I. Vermes, *J. Biomed. Biotechnol.* **2009**, 2009, 824148.
- [184] P. Cui, S. Wang, *J. Pharm. Anal.* **2019**, 9, 238.
- [185] L. R. Volpatti, A. K. Yetisen, *Trends Biotechnol.* **2014**, 32, 347.
- [186] K. F. Lei, *J. Lab. Autom.* **2012**, 17, 330.
- [187] B. Gale, A. Jafek, C. Lambert, B. Goenner, H. Moghimifam, U. Nze, S. Kamarapu, *Inventions* **2018**, 3, 60.
- [188] D. R. Seshadri, R. T. Li, J. E. Voos, J. R. Rowbottom, C. M. Alfes, C. A. Zorman, C. K. Drummond, *npj Digital Med.* **2019**, 2, 72.
- [189] J. R. Sempionatto, T. Nakagawa, A. Pavinatto, S. T. Mensah, S. Imani, P. Mercier, J. Wang, *Lab Chip* **2017**, 17, 1834.
- [190] M. Chung, G. Fortunato, N. Radacsi, *J. R. Soc., Interface* **2019**, 16, 20190217.
- [191] A. Nag, S. C. Mukhopadhyay, J. Kosel, *IEEE Sens. J.* **2017**, 17, 3949.
- [192] R. Mohammadzadeh Kakhki, *Arabian J. Chem.* **2019**, 12, 1783.
- [193] P. Takmakov, M. K. Zachek, R. B. Keithley, P. L. Walsh, C. Donley, G. S. McCarty, R. M. Wightman, *Anal. Chem.* **2010**, 82, 2020.
- [194] M. L. Huffman, B. J. Venton, *Analyst* **2009**, 134, 18.
- [195] A. Gonzalez-Pujana, E. Santos, G. Orive, J. L. Pedraz, R. M. Hernandez, *J. Drug Delivery Sci. Technol.* **2017**, 42, 49.
- [196] G. Orive, R. Maria Hernández, A. Rodríguez Gascón, R. Calafiore, T. M. Swi Chang, P. de Vos, G. Hortelano, D. Hunkeler, I. Lacík, J. Luis Pedraz, *Trends Biotechnol.* **2004**, 22, 87.
- [197] R. M. Olabisi, *J. Biomed. Mater. Res. Part A* **2015**, 103, 846.
- [198] Technavio, “Transdermal drug delivery market,” <https://www.technavio.com/report/transdermal-drug-delivery-market-industry-analysis?tnplus> (accessed: March 2022).
- [199] E. O’Day “Top 10 emerging technologies of 2020,” 2020, <https://www.weforum.org/reports/top-10-emerging-technologies-2020>, (accessed: December 2021).
- [200] K. Lee, J. Lee, S. G. Lee, S. Park, D. S. Yang, J.-J. Lee, A. Khademhosseini, J. S. Kim, W. Ryu, *J. Controlled Release* **2020**, 321, 174.
- [201] D.-H. Kim, J. B. Lee, M.-L. Kang, J. H. Park, J. You, S. Yu, J. Y. Park, S. B. Ryu, G. M. Seon, J.-K. Yoon, M. H. Lee, Y. M. Shin, K. D. Park, J.-C. Park, W. S. Jang, W. S. Kim, H.-J. Sung, *ACS Biomater. Sci. Eng.* **2018**, 4, 3848.
- [202] J. Domínguez-Robles, N. K. Martin, L. Fong, S. A. Stewart, N. J. Irwin, I. Rial-Hermida, R. F. Donnelly, E. Larrañeta, 2011, 11, 165.
- [203] A. G. Crişan, A. Porfire, R. Ambrus, G. Katona, L. M. Rus, A. S. Porav, K. Ilyés, I. Tomuţă, *Pharmaceuticals* **2021**, 14, 418.
- [204] F. Fina, A. Goyanes, S. Gaisford, A. W. Basit, *Int. J. Pharm.* **2017**, 529, 285.
- [205] M. Kirkby, A. R. J. Hutton, R. F. Donnelly, *Pharm. Res.* **2020**, 37, 117.
- [206] R. F. Donnelly, in *Microneedles for Drug and Vaccine Delivery and Patient Monitoring* (Eds: R. F. Donnelly, T. R. R. Singh, E. Larraneta, M. T. C. McCrudden), John Wiley & Sons, Ltd, Chichester, UK **2018**, pp. 307–322.
- [207] L. Wei-Ze, H. Mei-Rong, Z. Jian-Ping, Z. Yong-Qiang, H. Bao-Hua, L. Ting, Z. Yong, *Int. J. Pharm.* **2010**, 389, 122.
- [208] R. F. Donnelly, T. R. R. Singh, A. Z. Alkilani, M. T. C. McCrudden, S. O’Neill, C. O’Mahony, K. Armstrong, N. McLoone, P. Kole, A. D. Woolfson, *Int. J. Pharm.* **2013**, 451, 76.
- [209] “Regulatory Considerations for Microneedling Products | FDA,” 2020, <https://www.fda.gov/regulatory-information/search-fda-guidance-documents/regulatory-considerations-microneedling-products>, (accessed: March 2022).
- [210] R. F. Donnelly, A. D. Woolfson, *Ther. Delivery* **2014**, 5, 653.
- [211] F. R. Rozema, R. R. M. Bos, G. Boering, J. A. A. M. van Asten, A. J. Nijenhuis, A. J. Pennings, *J. Appl. Biomater.* **1991**, 2, 23.
- [212] D. K. Gilding, A. M. Reed, *Polymer* **1979**, 20, 1459.
- [213] R. Y. Neches, K. J. Flynn, L. Zaman, E. Tung, N. Pudlo, *PeerJ* **2016**, 4, e2661.
- [214] A. Ripolin, J. Quinn, E. Larrañeta, E. M. Vicente-Perez, J. Barry, R. F. Donnelly, *Int. J. Pharm.* **2017**, 521, 92.
- [215] C. K. Choi, J. B. Kim, E. H. Jang, Y.-N. Youn, W. H. Ryu, *Small* **2012**, 8, 2483.
- [216] Medicines & Healthcare products Regulatory Agency, “Patient Information Leaflet for COVID-19 Vaccine Janssen,” <https://www.gov.uk/government/publications/regulatory-approval-of-pfizer-biontech-vaccine-for-covid-19/patient-information-leaflet-for-covid-19-vaccine-pfizerbiontech> (accessed: March 2022).
- [217] M. & H. products R. Agency, “Information for UK recipients on Pfizer/BioNTech COVID-19 vaccine (Regulation 174) – GOV. UK,” <https://www.gov.uk/government/publications/regulatory-approval-of-pfizer-biontech-vaccine-for-covid-19/information-for-uk-recipients-on-pfizerbiontech-covid-19-vaccine> (accessed: March 2022).
- [218] N. C. for I. and R. D. (NCIRD) Centers for Disease Control and Prevention, “TABLE. Influenza vaccines — United States, 2021–22 influenza season* | CDC,” <https://www.cdc.gov/flu/professionals/acip/2021-2022/acip-table.htm> (accessed: March 2022).
- [219] J. Jiang, H. S. Gill, D. Ghate, B. E. McCarey, S. R. Patel, H. F. Edelhauser, M. R. Prausnitz, *Invest. Ophthalmol. Visual Sci.* **2007**, 48, 4038.
- [220] Y. Ma, S. E. Boese, Z. Luo, N. Nitin, H. S. Gill, *Biomed. Microdevices* **2015**, 17, 44.
- [221] J. A. Matriano, M. Cormier, J. Johnson, W. A. Young, M. BATTERY, K. Nyam, P. E. Daddona, *Pharm. Res.* **2002**, 19, 63.
- [222] A. K. Jain, C. H. Lee, H. S. Gill, *J. Controlled Release* **2016**, 239, 72.



Usanee Detamornrat is a research fellow at Queen's Belfast University. She received her M.Sc. degree in Drug Delivery from University College London (UCL) in 2015 and a Ph.D. degree in Pharmacy from the University of Nottingham in 2020. Her research focuses on drug delivery, disease diagnosis, and tissue engineering. She gained expertise in 3D printing, electrospinning, and microneedle technology during her studies. She has worked in collaboration with leading pharmaceutical and biotechnology companies.



Emma McAlister is a general practice pharmacist. Following completion of her Master's degree in Pharmacy (1st Class) and subsequently registering with the Pharmaceutical Society of Northern Ireland, she returned to Queen's University Belfast (QUB) to undertake a Ph.D. Her Ph.D. focused on the use of microneedles to transdermally deliver amoxicillin for the potential treatment of neonatal sepsis. Dr. McAlister then worked as a Research Fellow in QUB, developing MN-containing medical devices for patient monitoring and diagnostic testing. Dr. McAlister has currently published 12 research papers, 1 review paper, and 2 book chapters. She has presented her research at national/international conferences.



Aaron R. J. Hutton is a research fellow in the Donnelly lab within the School of Pharmacy, Queen's University Belfast. He received his Ph.D. from Queen's University Belfast in 2021. His Ph.D. involved the transdermal delivery of biomolecules using microarray patches alongside the development of patient feedback mechanisms using 3D printing technology. Through focused collaboration with industrial partners, Aaron is currently working on the upscale manufacturing and clinical translation of microarray patches.



Eneko Larrañeta is a senior lecturer at Queen's University Belfast. He graduated with a Ph.D. degree in Supramolecular Chemistry from the University of Navarra in 2012. He has published more than 50 papers, coedited a book, and published four book chapters. He has delivered multiple invited talks at conferences and international universities. He has attracted funding from EPSRC, Wellcome Trust, Academy of Medical Sciences, Society for Applied Microbiology and Royal Society. Additionally, he has worked in collaborative projects with leading pharmaceutical and cosmetics companies. Dr. Larrañeta is the author of a patent developed in collaboration with one of these companies.



Ryan F. Donnelly is a professor at Queen's University Belfast. He received his Ph.D. degree in Pharmaceutics from Queen's University Belfast in 2003. His research is focused on novel polymeric microneedle arrays for transdermal administration of "difficult-to-deliver" drugs and intradermal delivery of vaccines and photosensitizers. His work is funded by BBSRC, EPSRC, MRC, The Wellcome Trust, The Royal Society and the pharmaceutical and medical devices industries. He has authored over 600 peer-reviewed publications, including several granted patents, 6 textbooks and approximately 260 full papers. His work has attracted numerous awards, including the Academy of Pharmaceutical Sciences Innovative Science Award in 2020.